

# Supporting Information

## Sequence-Selective Binding of Oligopeptides in Water through Hydrophobic Coding

Joseph K. Awino, Roshan W. Gunasekara, and Yan Zhao\*

*Department of Chemistry, Iowa State University, Ames, Iowa 50011-3111, USA*

### Table of Contents

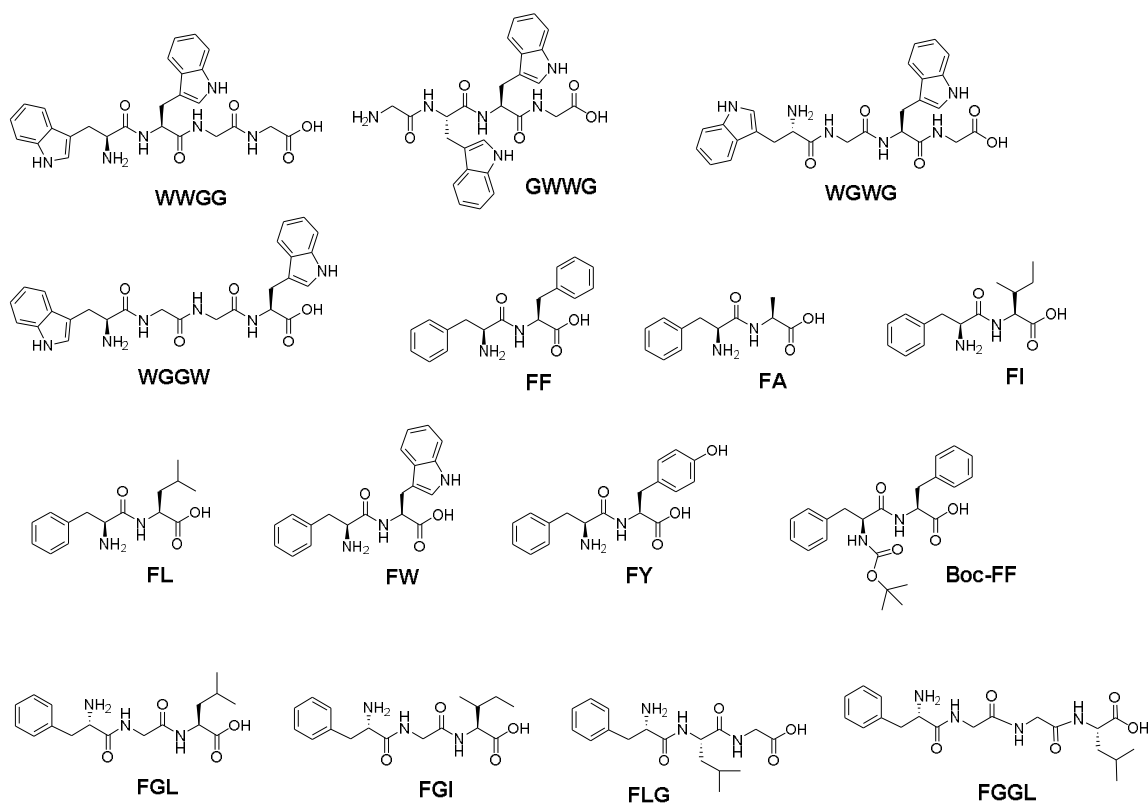
<i>General Method</i> .....	S3
<i>Chart S1</i> .....	S3
<i>Synthesis</i> .....	S4
Figure S1 .....	S5
Figure S2.....	S5
Figure S3 .....	S6
Figure S4 .....	S7
Figure S5.....	S7
Figure S6.....	S8
Figure S7 .....	S9
Figure S8.....	S9
Figure S9 .....	S10
Figure S10.....	S11
Figure S11.....	S11
Figure S12.....	S12
Figure S13.....	S13
Figure S14.....	S13
Figure S15.....	S14
Figure S16.....	S15
Figure S17.....	S15
Figure S18.....	S16
Figure S19.....	S17

Figure S20.....	S17
Figure S21.....	S18
Figure S22.....	S19
Figure S23.....	S19
Figure S24.....	S20
Figure S25.....	S21
Figure S26.....	S21
Figure S27.....	S22
Figure S28.....	S23
Figure S29.....	S23
Figure S30.....	S24
Figure S31.....	S25
Figure S32.....	S25
Figure S33.....	S26
Figure S34.....	S27
Figure S35.....	S27
Figure S36.....	S28
Figure S37.....	S29
Figure S38.....	S30
Figure S39.....	S31
Figure S40.....	S32
Figure S41.....	S32
Figure S42.....	S33
Figure S43.....	S33
Table S2.....	S34
Figure S44.....	S34
Figure S45.....	S35
Figure S46.....	S36
Figure S47.....	S37
Figure S48.....	S38
Figure S49.....	S39
Figure S50.....	S40
Figure S51.....	S41
Figure S52.....	S42
Figure S53.....	S43

## General Method

Adrenocorticotrophic hormone (ACTH),  $\beta$ -amyloid, kassinin, glucagon, and octreotide were purchased from GenScript USA Inc., and reconstituted according to the instructions. Other oligopeptides were purchased from GL Biochem (Shanghai) Ltd. All other reagents and solvents were of ACS-certified grade or higher, and were used as received from the commercial suppliers. Routine  $^1\text{H}$  and  $^{13}\text{C}$  NMR spectra were recorded on a Bruker DRX-400 or on a Varian VXR-400 spectrometer. ESI-MS mass was recorded on Shimadzu LCMS-2010 mass spectrometer. Fluorescence spectra were recorded at ambient temperature on a Varian Cary Eclipse Fluorescence spectrophotometer. ITC was performed using a MicroCal VP-ITC Microcalorimeter with Origin 7 software and VPViewer2000 (GE Healthcare, Northampton, MA).

**Chart S1.** Structures of peptides used in the study.



## *Synthesis*

**Typical procedure for the synthesis of MINPs.**<sup>1</sup> To a micellar solution of compound **1** (9.3 mg, 0.02 mmol) in D<sub>2</sub>O (2.0 mL), divinylbenzene (DVB, 2.8 μL, 0.02 mmol), WWGG (10 μL of a 21.1 mg/mL, 0.0004 mmol) in D<sub>2</sub>O, and 2,2-dimethoxy-2-phenylacetophenone (DMPA, 10 μL of a 12.8 mg/mL, 0.0005 mmol) in DMSO were added. (D<sub>2</sub>O instead of H<sub>2</sub>O was used to allow the reaction progress to be monitored by <sup>1</sup>H NMR spectroscopy.) The mixture was subjected to ultrasonication for 10 min before compound **2** (4.1 mg, 0.024 mmol), CuCl<sub>2</sub> (10 μL of a 6.7 mg/mL, 0.0005 mmol) in D<sub>2</sub>O, and sodium ascorbate (10 μL of a 99 mg/mL solution, 0.005 mmol) in D<sub>2</sub>O were added. After the reaction mixture was stirred slowly at room temperature for 12 h, compound **3** (10.6 mg, 0.04 mmol), CuCl<sub>2</sub> (10 μL of a 6.7 mg/mL solution, 0.0005 mmol), and sodium ascorbate (10 μL of a 99 mg/mL solution, 0.005 mmol) in D<sub>2</sub>O were added. The reaction mixture was stirred for another 6 h at room temperature and transferred to a glass vial, purged with nitrogen for 15 min, then sealed with a rubber stopper and irradiated in a Rayonet reactor for 12 h. <sup>1</sup>H NMR spectroscopy was used to monitor the progress of reaction. The reaction mixture was poured into acetone (8 mL). The precipitate was collected by centrifugation and washed with a mixture of acetone/water (5 mL/1 mL) three times, followed by methanol/acetic acid (5 mL/0.1 mL) three times. The product was dried in air to afford the final MINPs (~80%).

---

<sup>1</sup> Awino, J. K.; Zhao, Y. *J. Am. Chem. Soc.* **2013**, *135*, 12552.

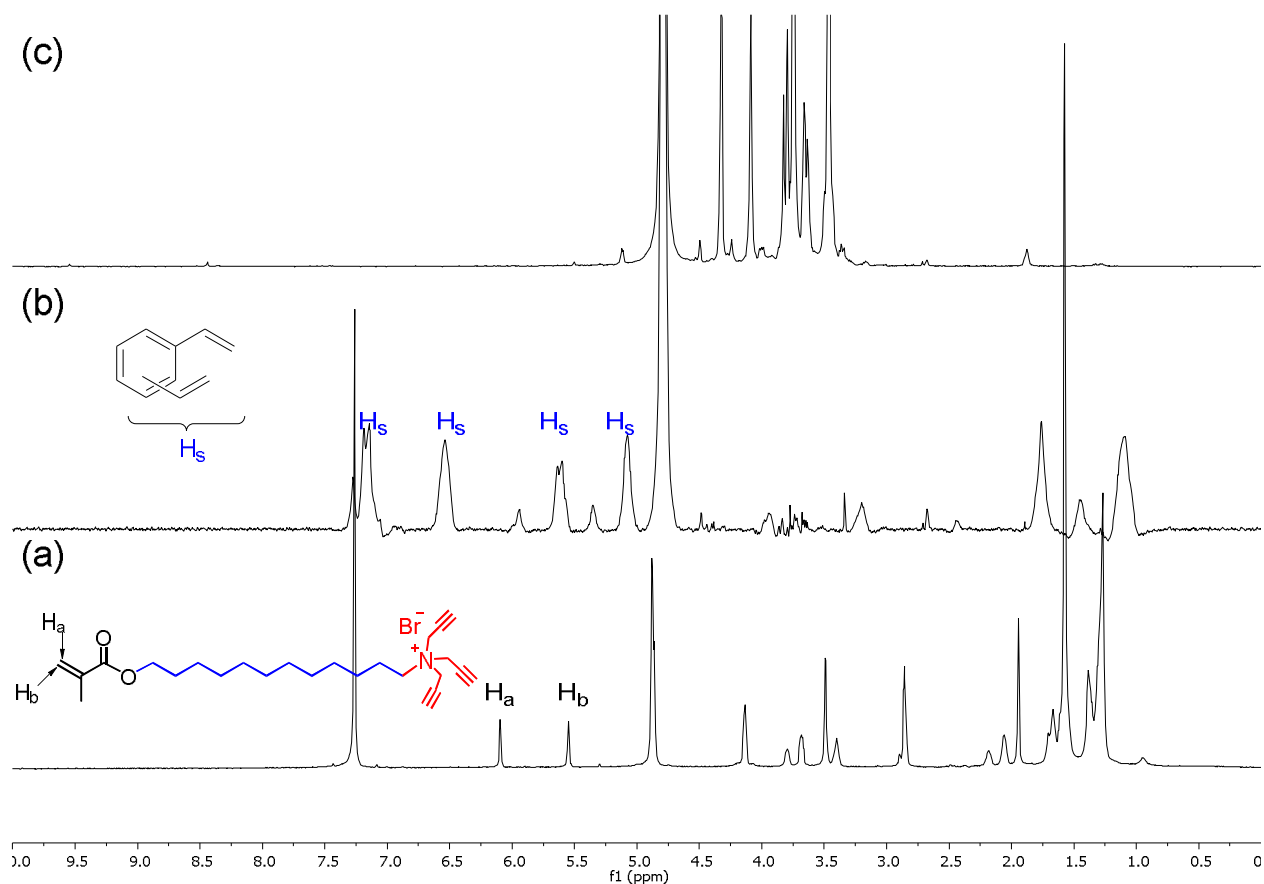


**Figure S1.**  $^1\text{H}$  NMR spectra of (a) Compound 1 in  $\text{CDCl}_3$ , (b) alkyne-SCM in  $\text{D}_2\text{O}$ , and (c) MINP(WWGG) in  $\text{D}_2\text{O}$ .

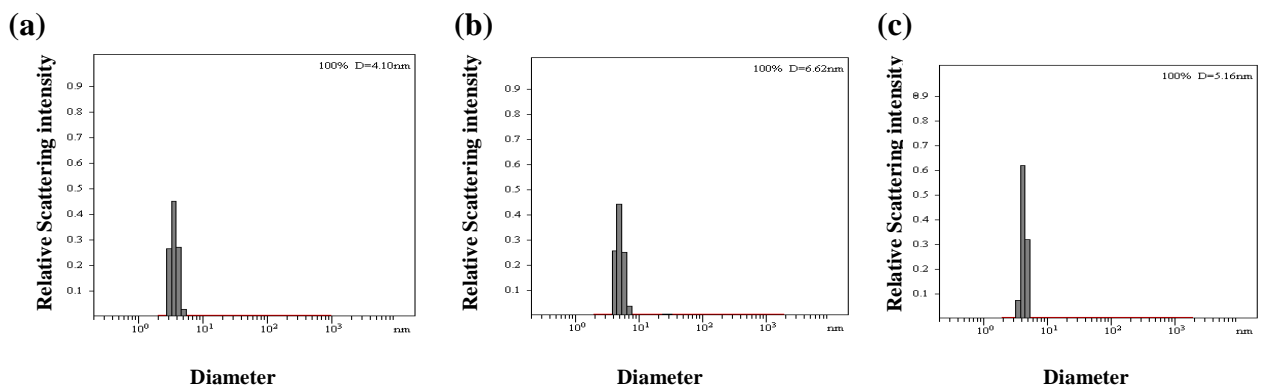


**Figure S2.** Distribution of the hydrodynamic diameters of the nanoparticles in water as determined by DLS for (a) alkyne-SCM, (b) surface-functionalized SCM, and (c) MINP(WWGG) after purification.

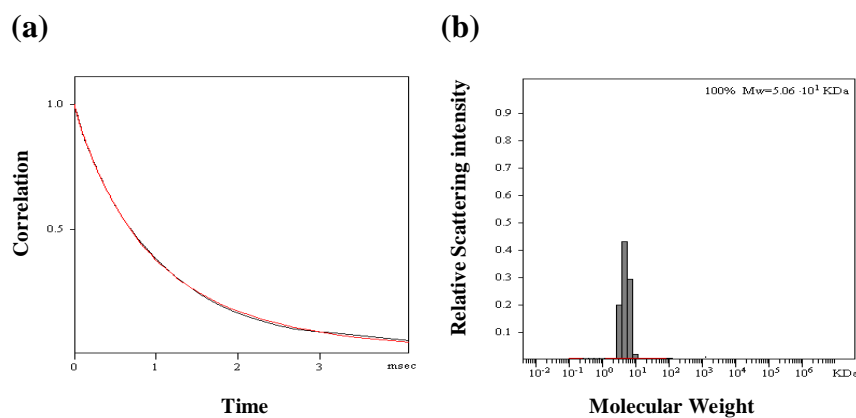


**Figure S3.** Distribution of the molecular weights and the correlation curves for MINP(WWGG) from the DLS. The PRECISION DECONVOLVE program assumes the intensity of scattering is proportional to the mass of the particle squared. If each unit of building block for the MINP(WWGG) is assumed to contain one molecule of compound **1** (MW = 465 g/mol), 1.2 molecules of compound **2** (MW = 172 g/mol), one molecule of DVB (MW = 130 g/mol), and 0.8 molecules of compound **3** (MW = 264 g/mol), the molecular weight of MINP(WWGG) translates to 50 [= 50600 / (465 + 1.2×172 + 130 + 0.8×264)] of such units.

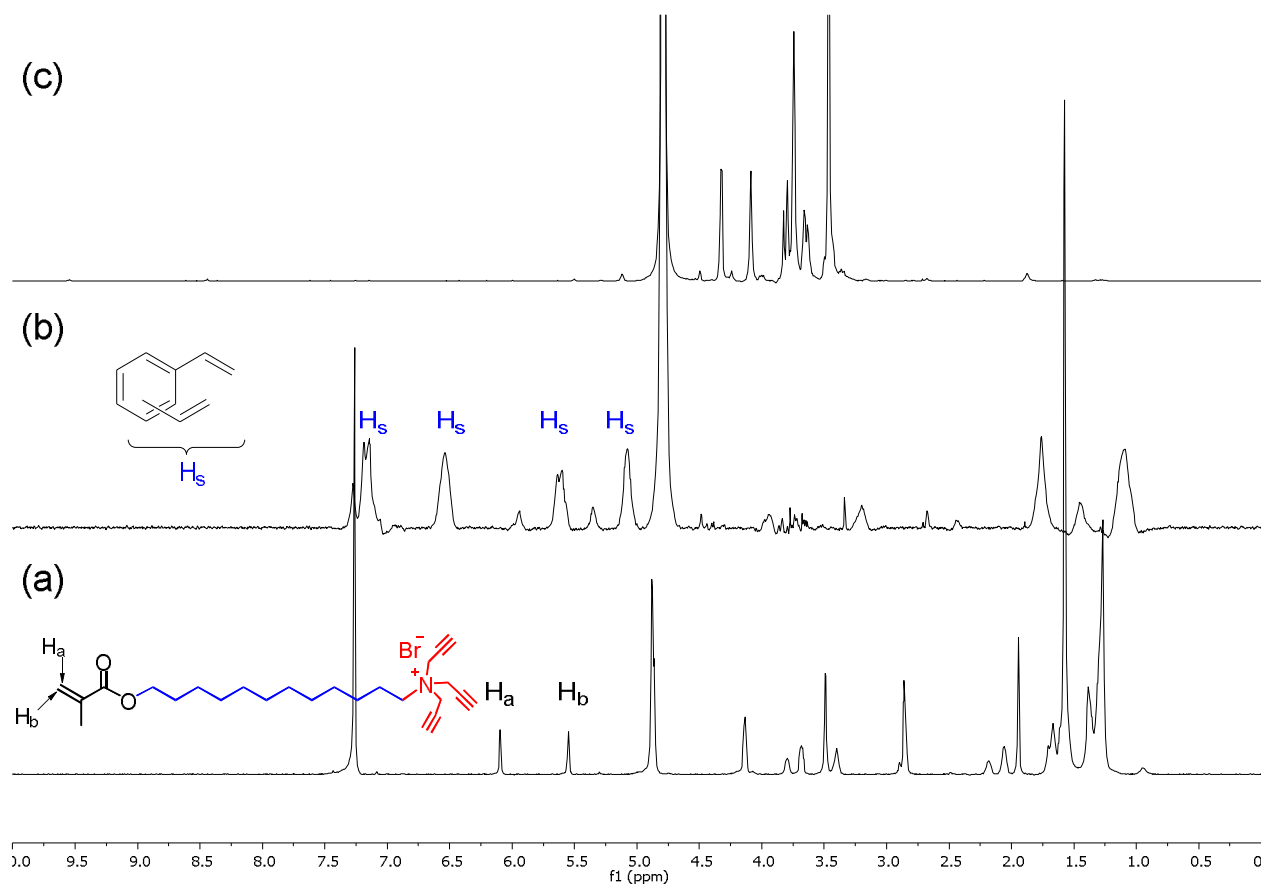


**Figure S4.** <sup>1</sup>H NMR spectra of (a) Compound 1 in CDCl<sub>3</sub>, (b) alkyne-SCM in D<sub>2</sub>O, and (c) MINP(GWWG) in D<sub>2</sub>O.

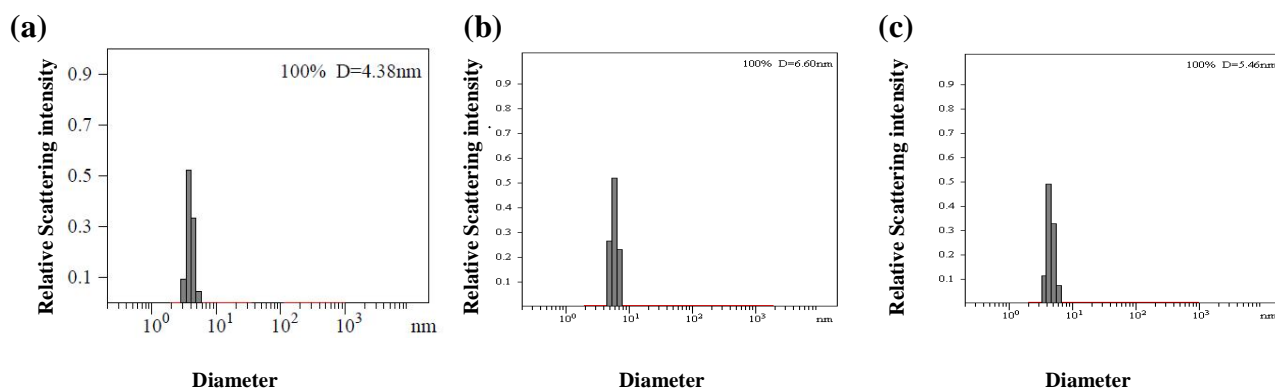


**Figure S5.** Distribution of the hydrodynamic diameters of the nanoparticles in water as determined by DLS for (a) alkyne-SCM, (b) surface-functionalized SCM, and (c) MINP(GWWG) after purification.

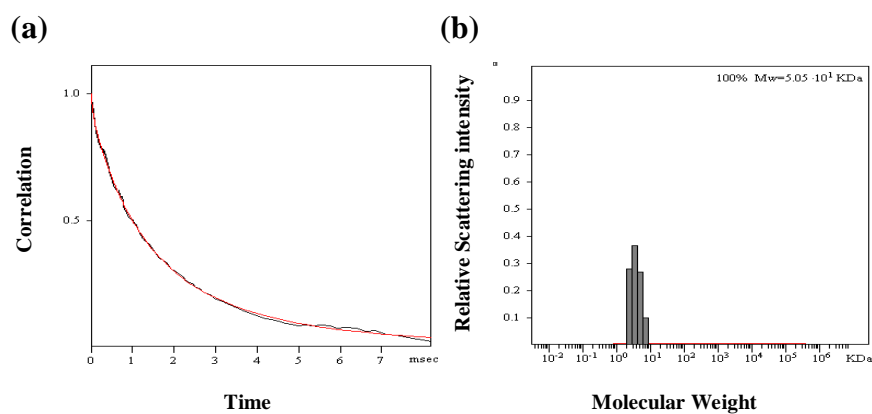


**Figure S6.** Distribution of the molecular weights and the correlation curves for MINP(GWWG) from the DLS. The PRECISION DECONVOLVE program assumes the intensity of scattering is proportional to the mass of the particle squared. If each unit of building block for the MINP(GWWG) is assumed to contain one molecule of compound **1** (MW = 465 g/mol), 1.2 molecules of compound **2** (MW = 172 g/mol), one molecule of DVB (MW = 130 g/mol), and 0.8 molecules of compound **3** (MW = 264 g/mol), the molecular weight of MINP(GWWG) translates to 50 [= 50500 / (465 + 1.2×172 + 130 + 0.8×264)] of such units.

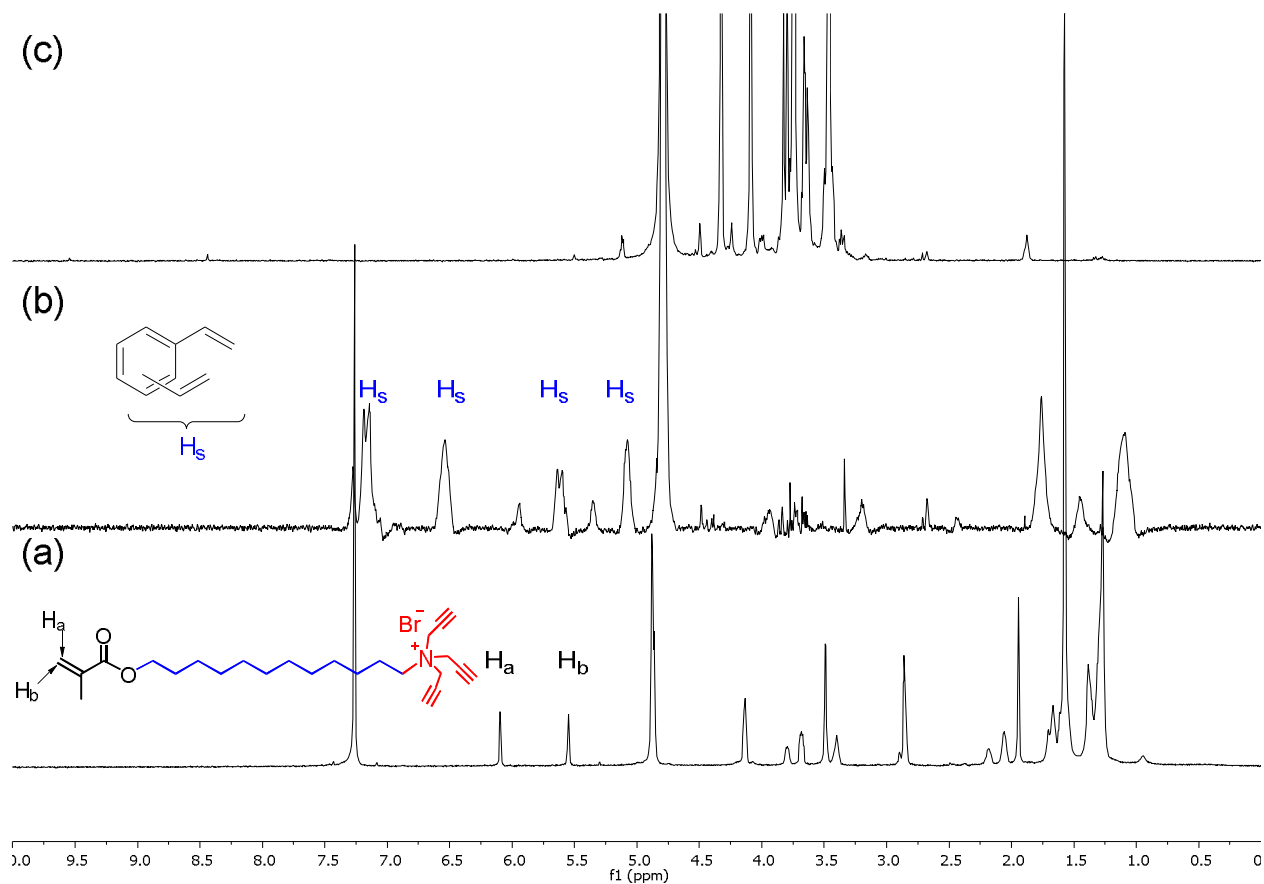


**Figure S7.**  $^1\text{H}$  NMR spectra of (a) Compound 1 in  $\text{CDCl}_3$ , (b) alkyne-SCM in  $\text{D}_2\text{O}$ , and (c) MINP(WGWW) in  $\text{D}_2\text{O}$ .

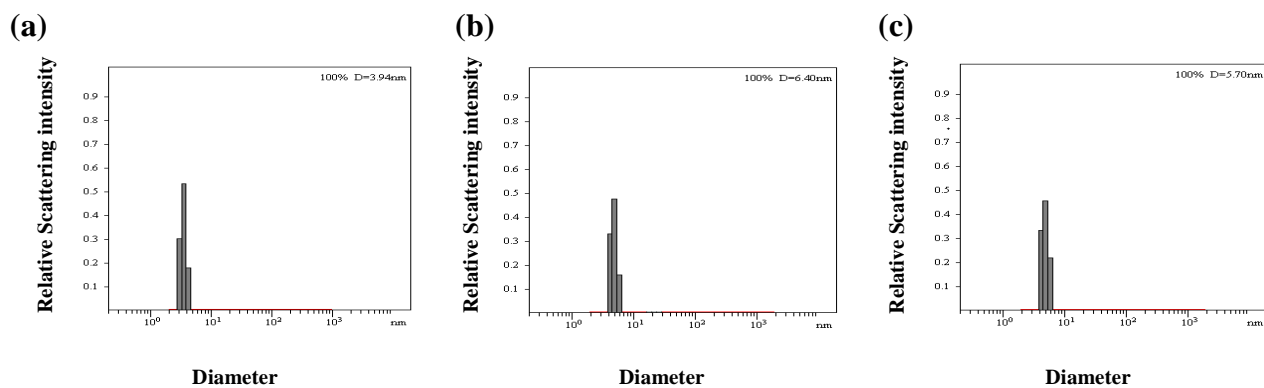


**Figure S8.** Distribution of the hydrodynamic diameters of the nanoparticles in water as determined by DLS for (a) alkyne-SCM, (b) surface-functionalized SCM, and (c) MINP(WGWW) after purification.

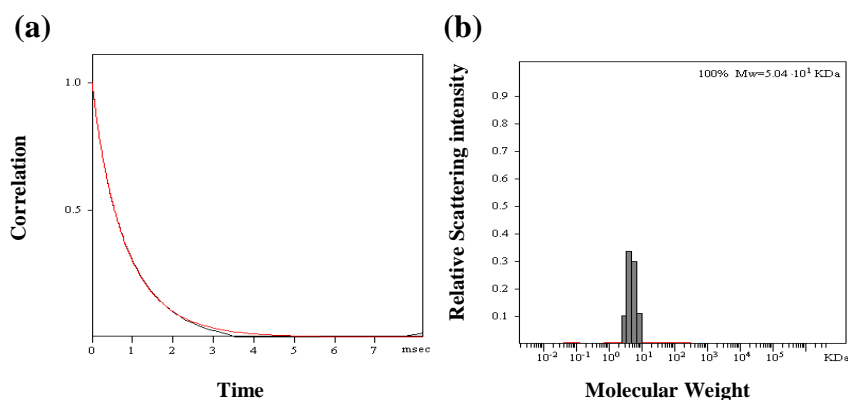


**Figure S9.** Distribution of the molecular weights and the correlation curves for MINP(WG WG) from the DLS. The PRECISION DECONVOLVE program assumes the intensity of scattering is proportional to the mass of the particle squared. If each unit of building block for the MINP(WG WG) is assumed to contain one molecule of compound **1** (MW = 465 g/mol), 1.2 molecules of compound **2** (MW = 172 g/mol), one molecule of DVB (MW = 130 g/mol), and 0.8 molecules of compound **3** (MW = 264 g/mol), the molecular weight of MINP(WG WG) translates to 50 [=  $50400 / (465 + 1.2 \times 172 + 130 + 0.8 \times 264)$ ] of such units.

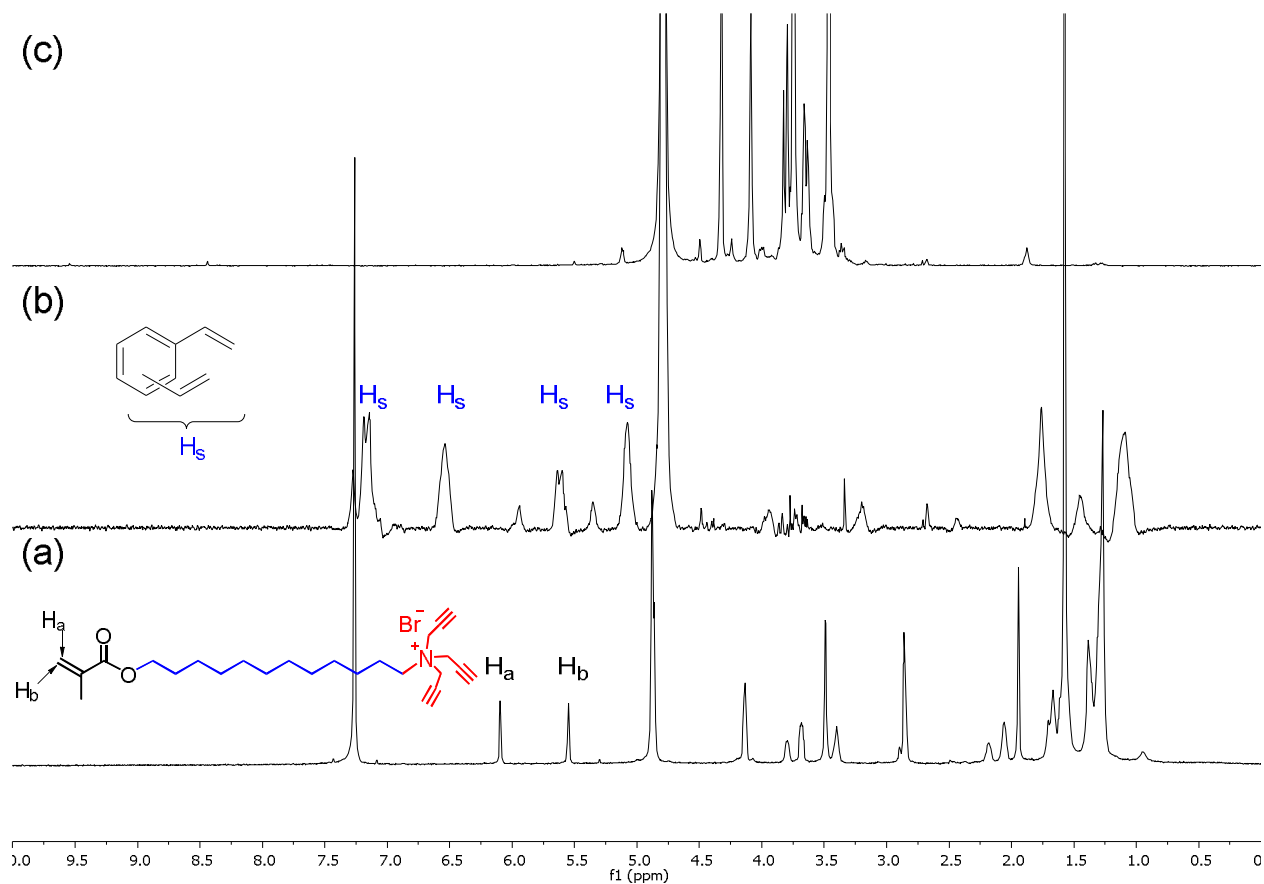


**Figure S10.**  $^1\text{H}$  NMR spectra of (a) Compound **1** in  $\text{CDCl}_3$ , (b) alkyne-SCM in  $\text{D}_2\text{O}$ , and (c) MINP(WGGW) in  $\text{D}_2\text{O}$ .

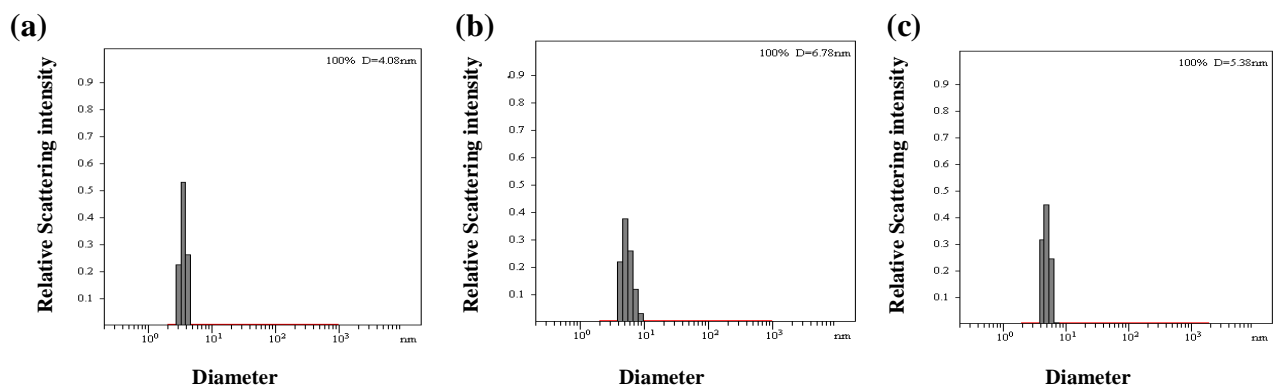


**Figure S11.** Distribution of the hydrodynamic diameters of the nanoparticles in water as determined by DLS for (a) alkyne-SCM, (b) surface-functionalized SCM, and (c) MINP(WGGW) after purification.

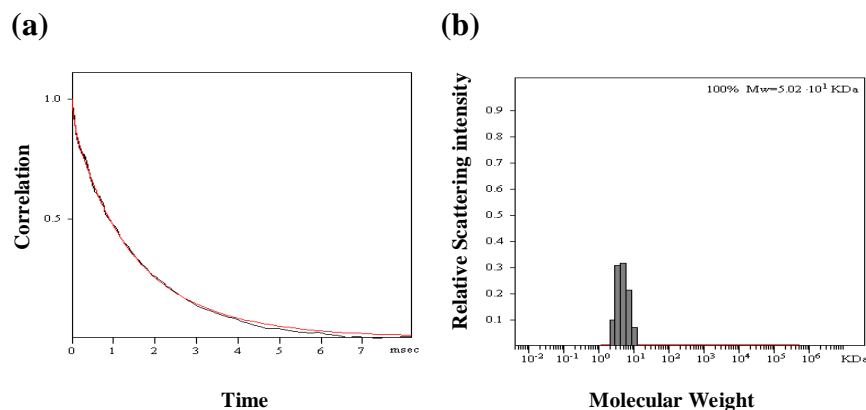


**Figure S12.** Distribution of the molecular weights and the correlation curves for MINP(WGGW) from the DLS. The PRECISION DECONVOLVE program assumes the intensity of scattering is proportional to the mass of the particle squared. If each unit of building block for the MINP(WGGW) is assumed to contain one molecule of compound **1** (MW = 465 g/mol), 1.2 molecules of compound **2** (MW = 172 g/mol), one molecule of DVB (MW = 130 g/mol), and 0.8 molecules of compound **3** (MW = 264 g/mol), the molecular weight of MINP(WGGW) translates to 50 [= 50200 / (465 + 1.2×172 + 130 + 0.8×264)] of such units.

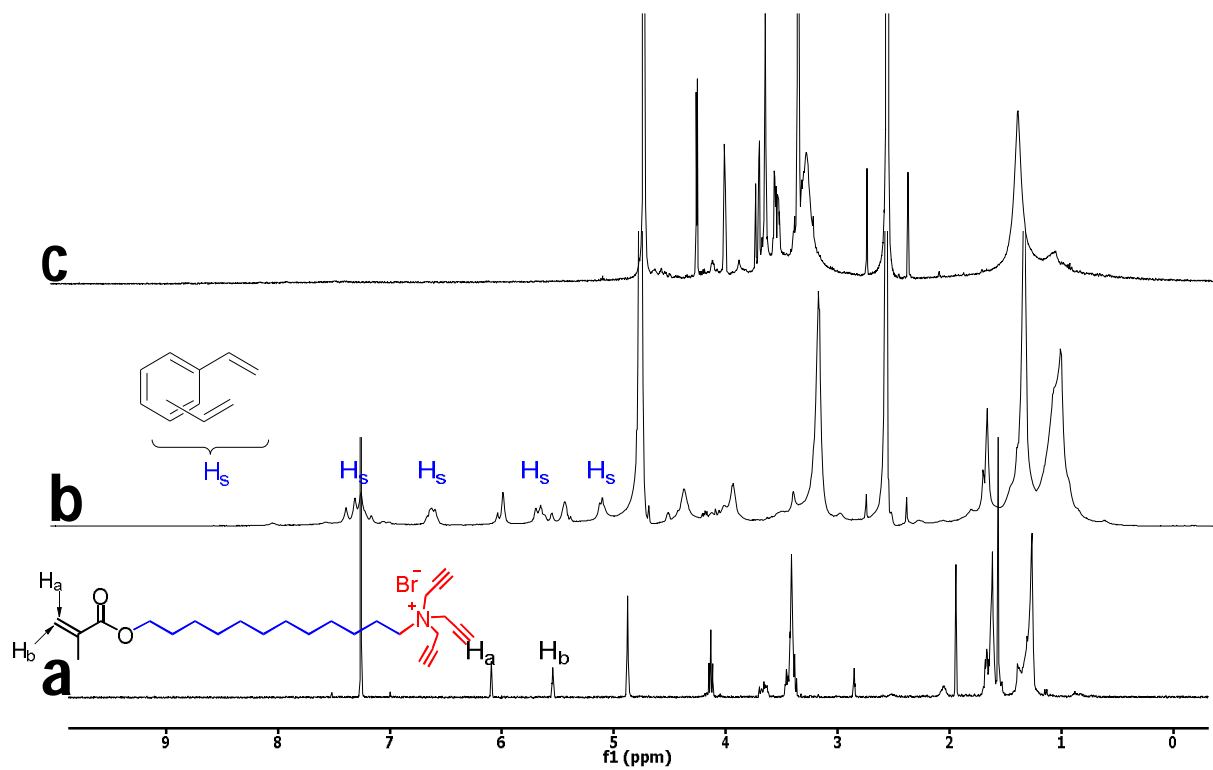


**Figure S13.**  $^1\text{H}$  NMR spectra of (a) Compound **1** in  $\text{CDCl}_3$ , (b) alkynyl-SCM in  $\text{D}_2\text{O}$ , and (c) MINP(Boc-FF) in  $\text{D}_2\text{O}$ .

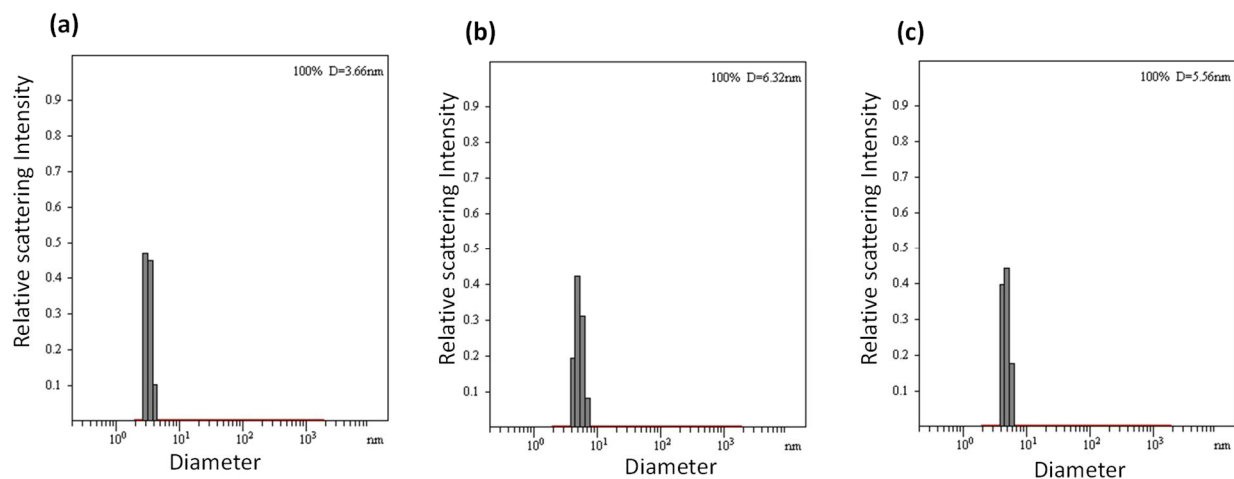


**Figure S14.** Distribution of the hydrodynamic diameters of the nanoparticles in water as determined by DLS for (a) alkynyl-SCM, (b) surface-functionalized SCM, and (c) MINP(Boc-FF) after purification.

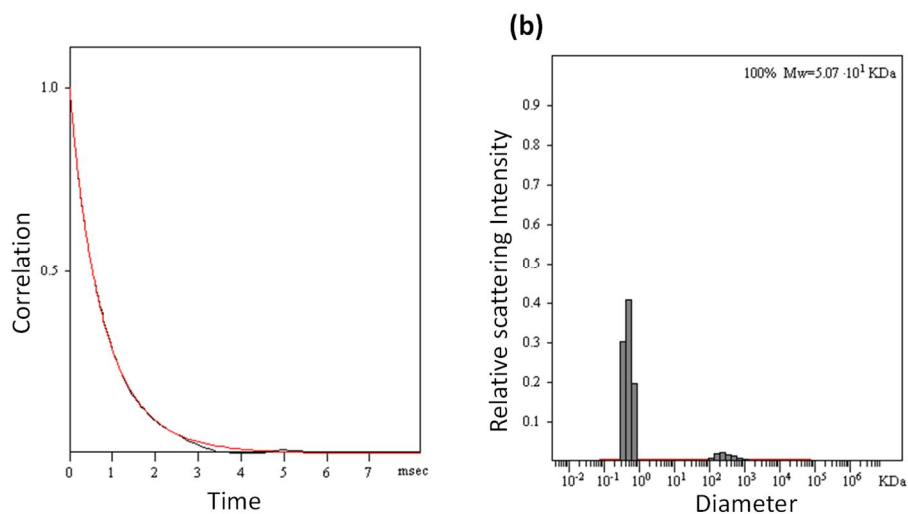


**Figure S15.** Distribution of the molecular weights and the correlation curves for MINP(Boc-FF) from the DLS. The PRECISION DECONVOLVE program assumes the intensity of scattering is proportional to the mass of the particle squared. If each unit of building block for the MINP(Boc-FF) is assumed to contain one molecule of compound **1** (MW = 465 g/mol), 1.2 molecules of compound **2** (MW = 172 g/mol), one molecule of DVB (MW = 130 g/mol), and 0.8 molecules of compound **3** (MW = 264 g/mol), the molecular weight of MINP(Boc-FF) translates to 50 [= 50700 / (465 + 1.2×172 + 130 + 0.8×264)] of such units.

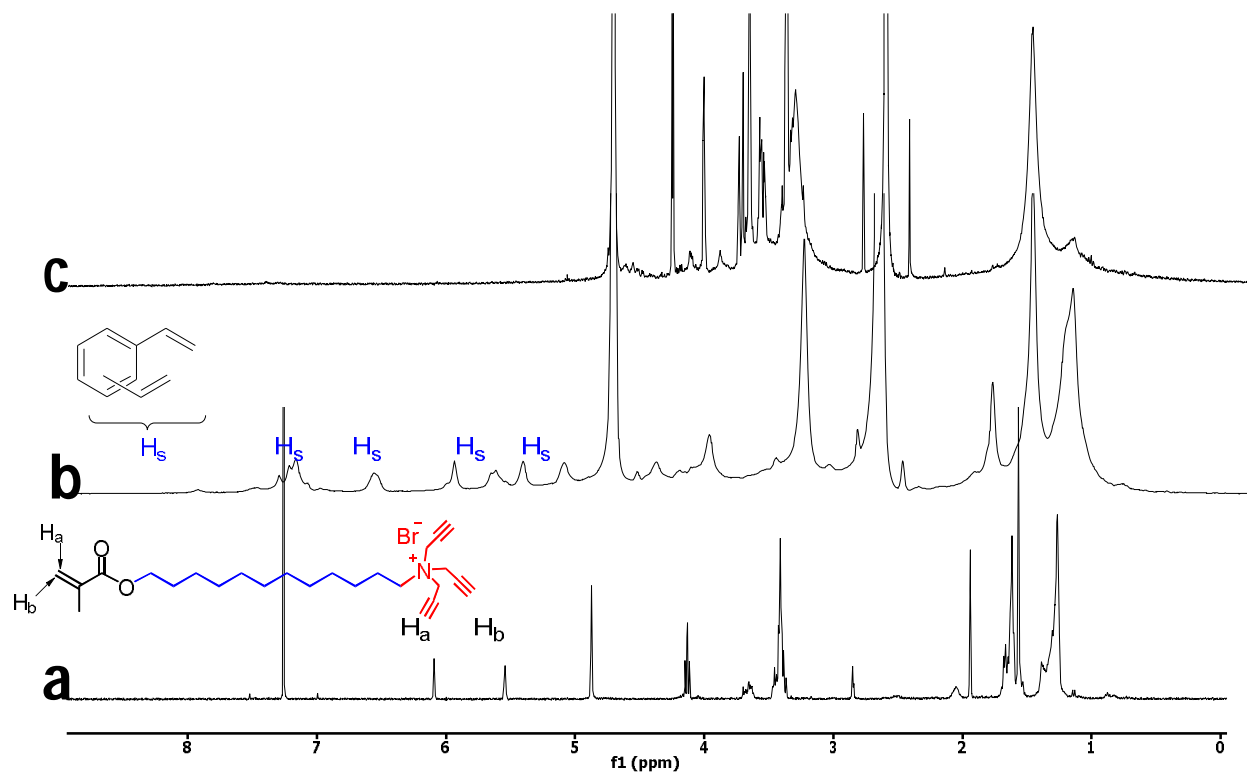


**Figure S16.**  $^1\text{H}$  NMR spectra of (a) Compound 1 in  $\text{CDCl}_3$ , (b) alkynyl-SCM in  $\text{D}_2\text{O}$ , and (c) MINP(FF) in  $\text{D}_2\text{O}$ .

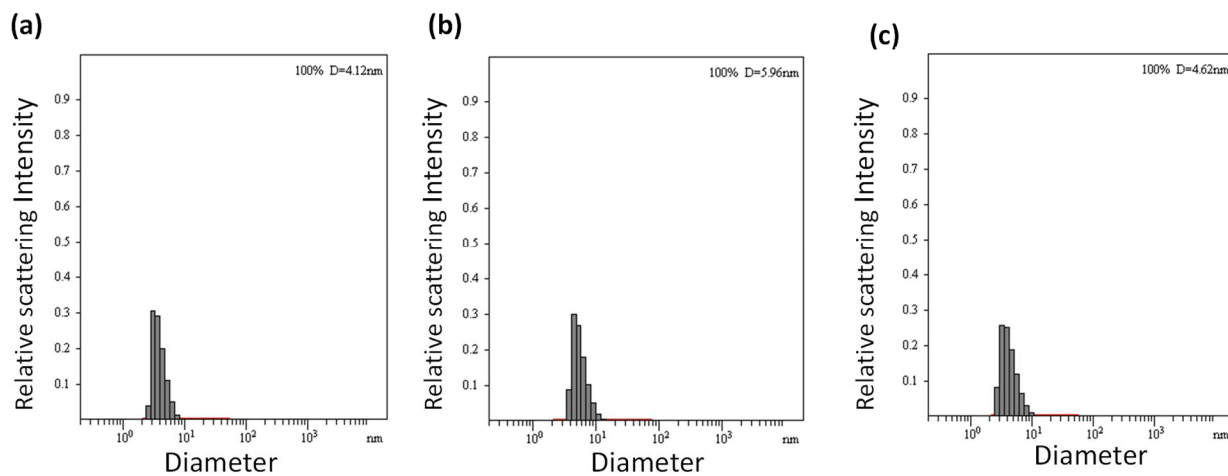


**Figure S17.** Distribution of the hydrodynamic diameters of the nanoparticles in water as determined by DLS for (a) alkynyl-SCM, (b) surface-functionalized SCM, and (c) MINP(FF) after purification.

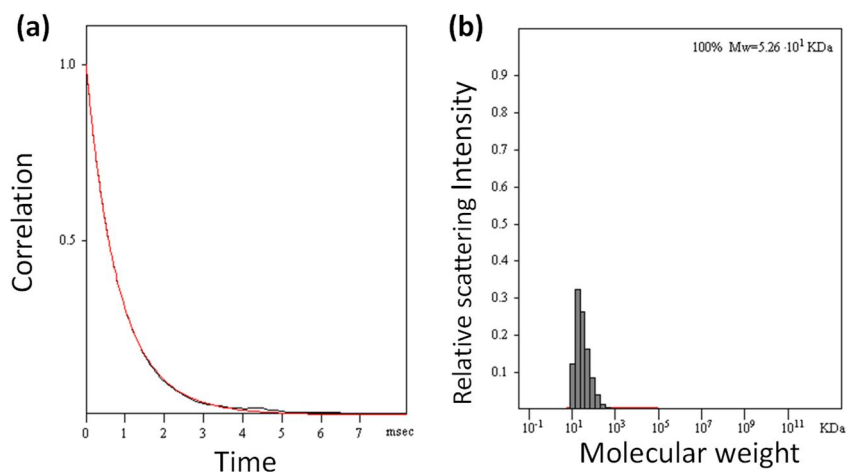


**Figure S18.** Distribution of the molecular weights and the correlation curves for MINP(FF) from the DLS. The PRECISION DECONVOLVE program assumes the intensity of scattering is proportional to the mass of the particle squared. If each unit of building block for the MINP(FF) is assumed to contain one molecule of compound **1** (MW = 465 g/mol), 1.2 molecules of compound **2** (MW = 172 g/mol), one molecule of DVB (MW = 130 g/mol), and 0.8 molecules of compound **3** (MW = 264 g/mol), the molecular weight of MINP(FF) translates to 52 [= 52600 / (465 + 1.2×172 + 130 + 0.8×264)] of such units.

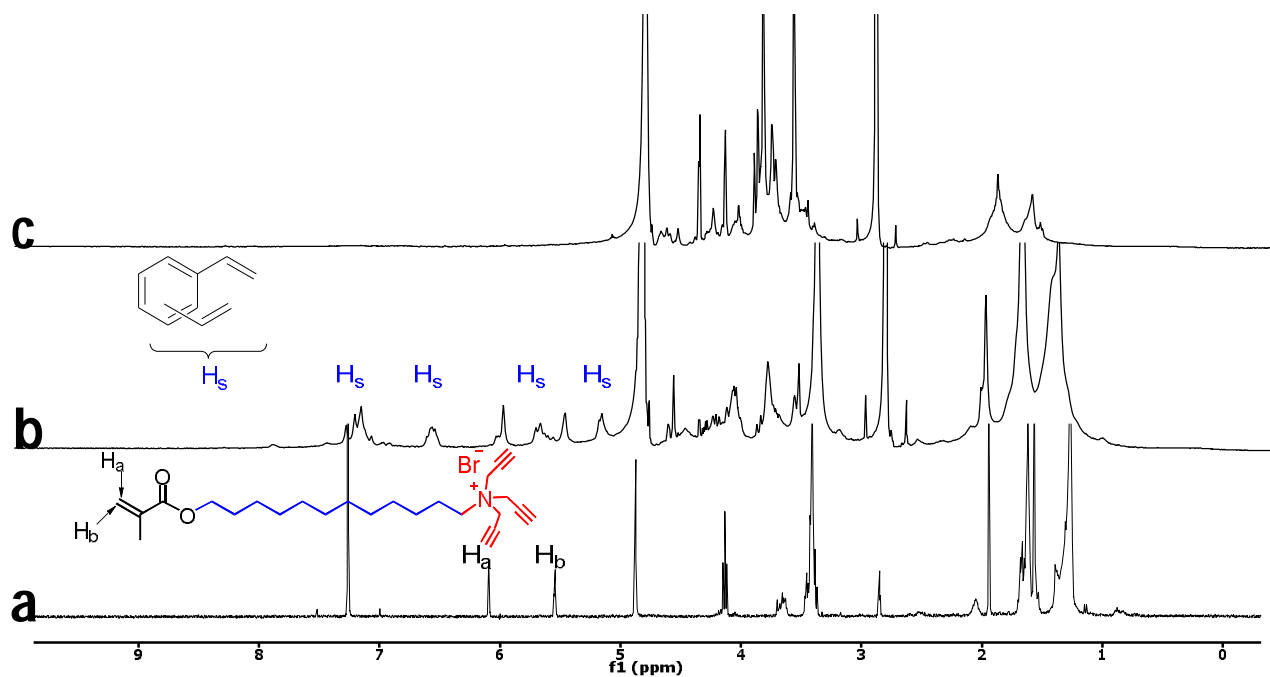


**Figure S19.**  $^1\text{H}$  NMR spectra of (a) Compound **1** in  $\text{CDCl}_3$ , (b) alkynyl-SCM in  $\text{D}_2\text{O}$ , and (c) MINP(FGL) in  $\text{D}_2\text{O}$ .

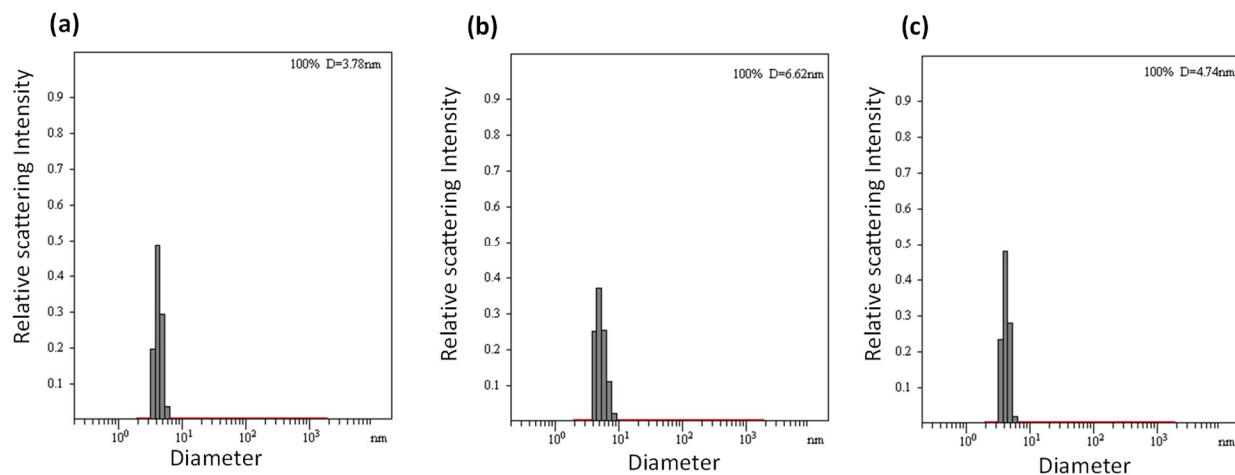


**Figure S20.** Distribution of the hydrodynamic diameters of the nanoparticles in water as determined by DLS for (a) alkynyl-SCM, (b) surface-functionalized SCM, and (c) MINP(FGL) after purification.

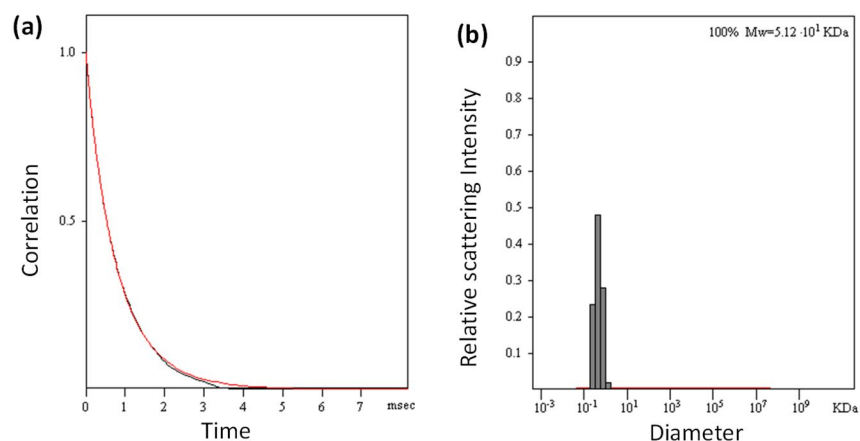


**Figure S21.** Distribution of the molecular weights and the correlation curves for MINP(FGL) from the DLS. The PRECISION DECONVOLVE program assumes the intensity of scattering is proportional to the mass of the particle squared. If each unit of building block for the MINP(FGL) is assumed to contain one molecule of compound **1** (MW = 465 g/mol), 1.2 molecules of compound **2** (MW = 172 g/mol), one molecule of DVB (MW = 130 g/mol), and 0.8 molecules of compound **3** (MW = 264 g/mol), the molecular weight of MINP(FGL) translates to 51 [= 51200 / (465 + 1.2×172 + 130 + 0.8×264)] of such units.

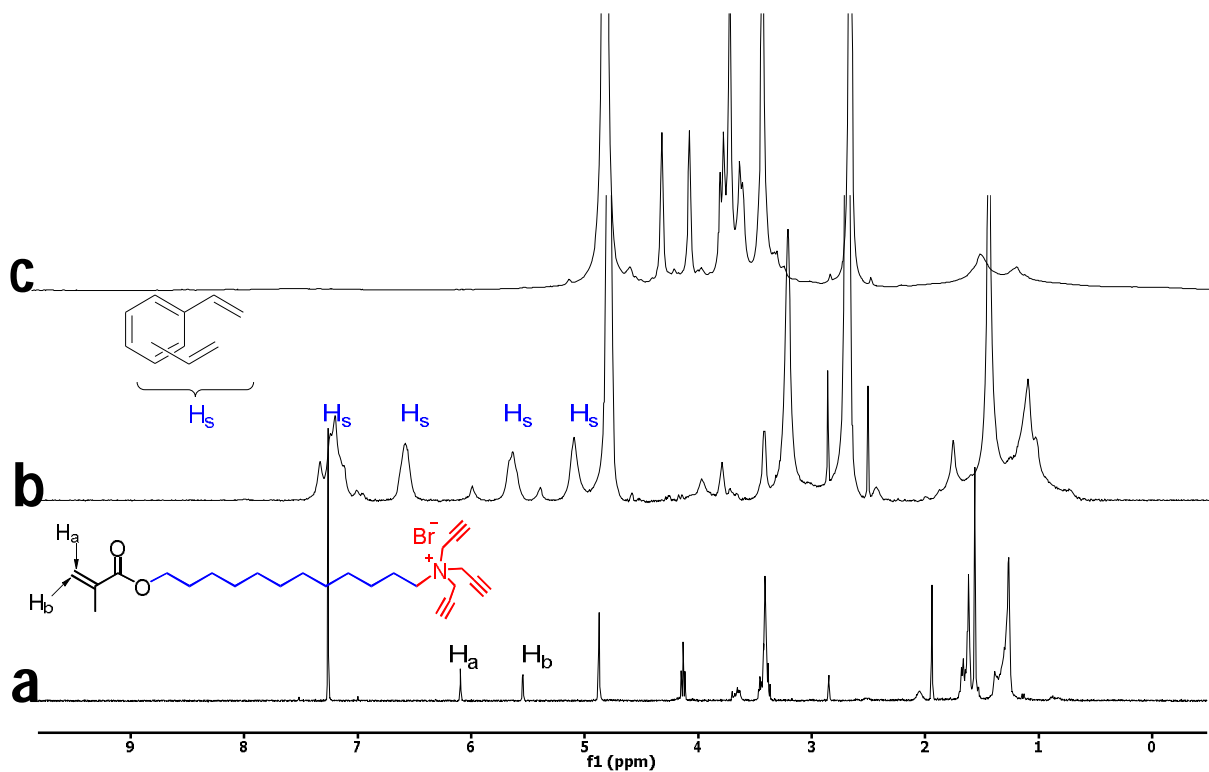


**Figure S22.**  $^1\text{H}$  NMR spectra of (a) Compound **1** in  $\text{CDCl}_3$ , (b) alkynyl-SCM in  $\text{D}_2\text{O}$ , and (c) MINP(**4**) in  $\text{D}_2\text{O}$ .

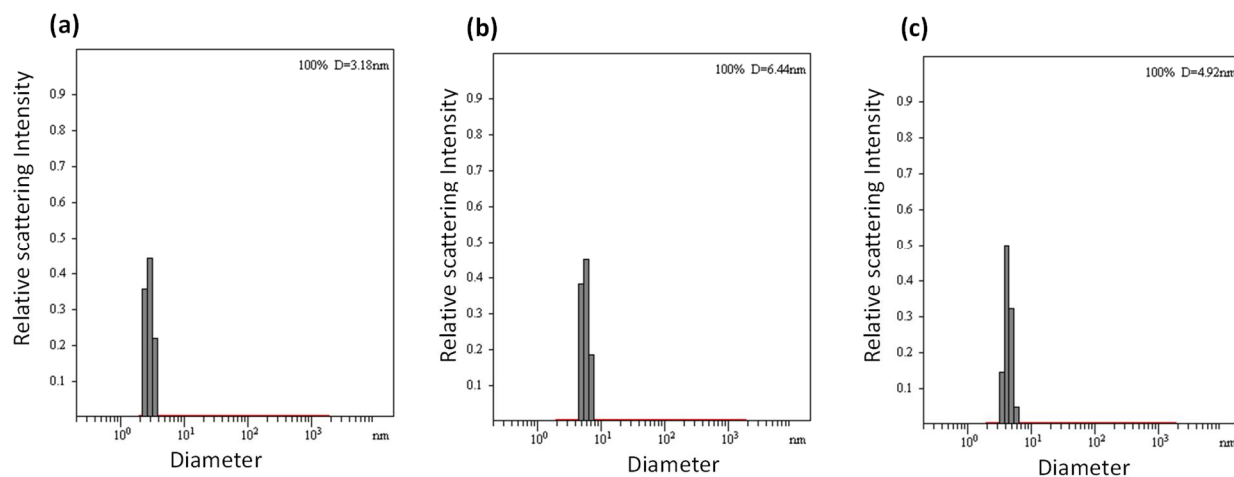


**Figure S23.** Distribution of the hydrodynamic diameters of the nanoparticles in water as determined by DLS for (a) alkynyl-SCM, (b) surface-functionalized SCM, and (c) MINP(**4**) after purification.

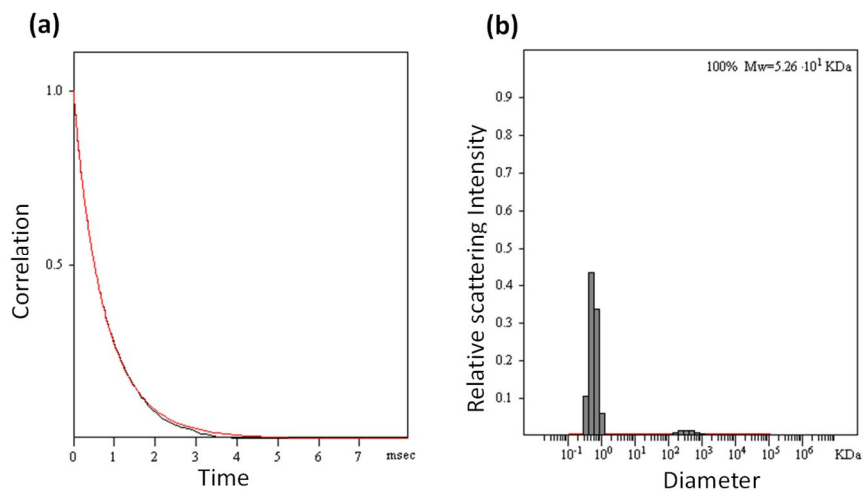


**Figure S24.** Distribution of the molecular weights and the correlation curves for MINP(4) from the DLS. The PRECISION DECONVOLVE program assumes the intensity of scattering is proportional to the mass of the particle squared. If each unit of building block for the MINP(4) is assumed to contain one molecule of compound **1** (MW = 465 g/mol), 1.2 molecules of compound **2** (MW = 172 g/mol), one molecule of DVB (MW = 130 g/mol), and 0.8 molecules of compound **3** (MW = 264 g/mol), the molecular weight of MINP(4) translates to 52 [= 52600 / (465 + 1.2×172 + 130 + 0.8×264)] of such units.

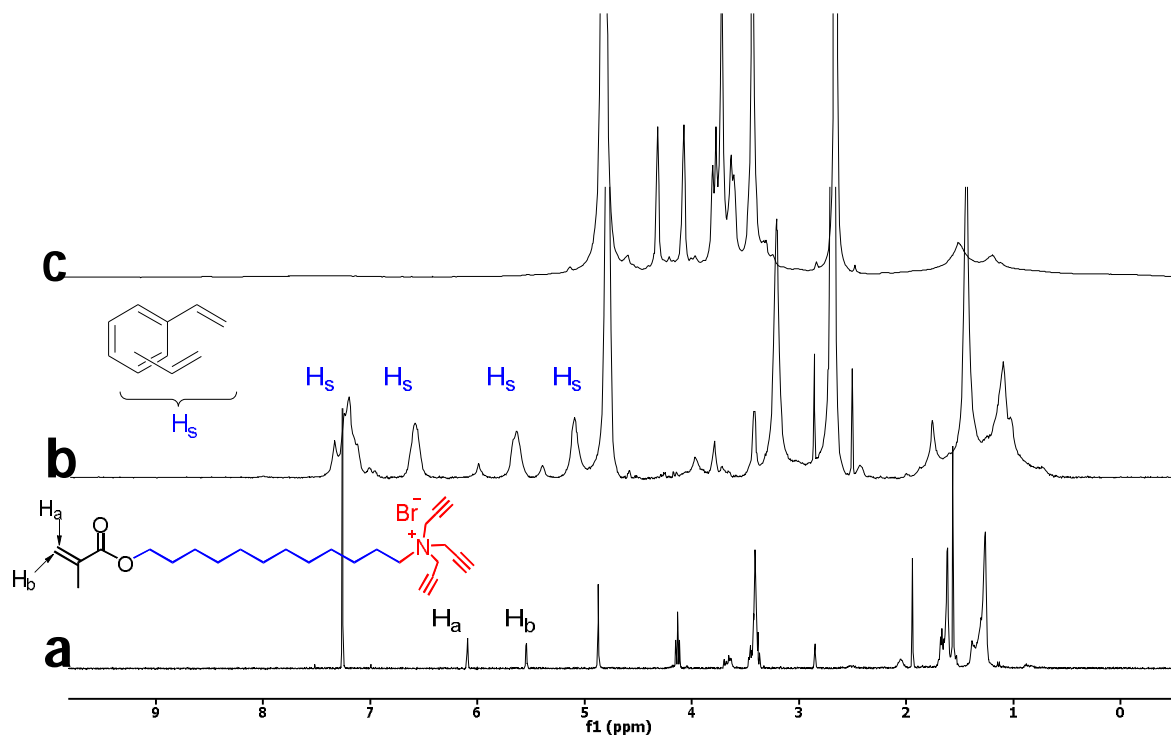


**Figure S25.**  $^1\text{H}$  NMR spectra of (a) Compound **1** in  $\text{CDCl}_3$ , (b) alkynyl-SCM in  $\text{D}_2\text{O}$ , and (c) MINP(**5**) in  $\text{D}_2\text{O}$ .

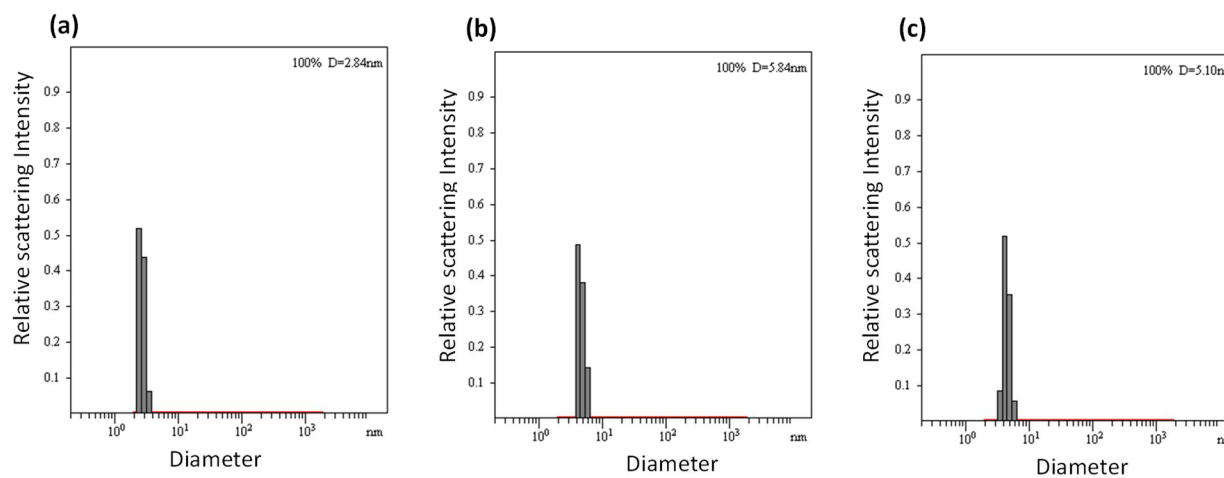


**Figure S26.** Distribution of the hydrodynamic diameters of the nanoparticles in water as determined by DLS for (a) alkynyl-SCM, (b) surface-functionalized SCM, and (c) MINP(**5**) after purification.

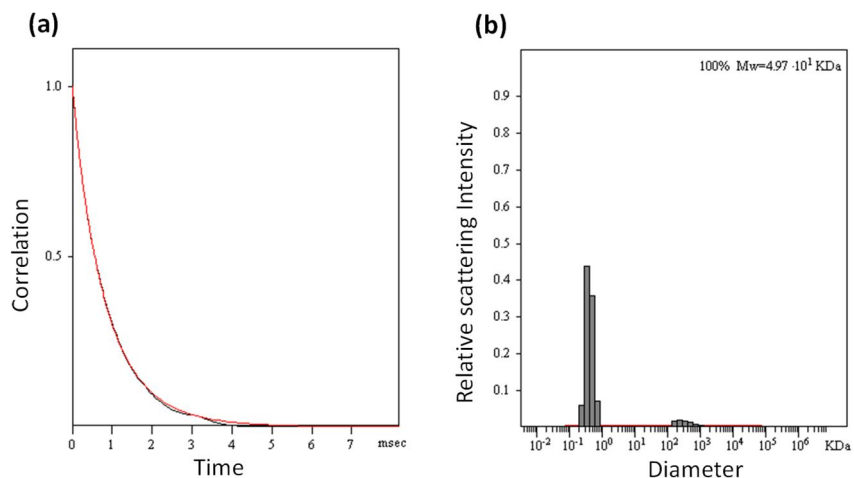


**Figure S27.** Distribution of the molecular weights and the correlation curves for MINP(**5**) from the DLS. The PRECISION DECONVOLVE program assumes the intensity of scattering is proportional to the mass of the particle squared. If each unit of building block for the MINP(**5**) is assumed to contain one molecule of compound **1** (MW = 465 g/mol), 1.2 molecules of compound **2** (MW = 172 g/mol), one molecule of DVB (MW = 130 g/mol), and 0.8 molecules of compound **3** (MW = 264 g/mol), the molecular weight of MINP(**5**) translates to 49 [=  $49700 / (465 + 1.2 \times 172 + 130 + 0.8 \times 264)$ ] of such units.

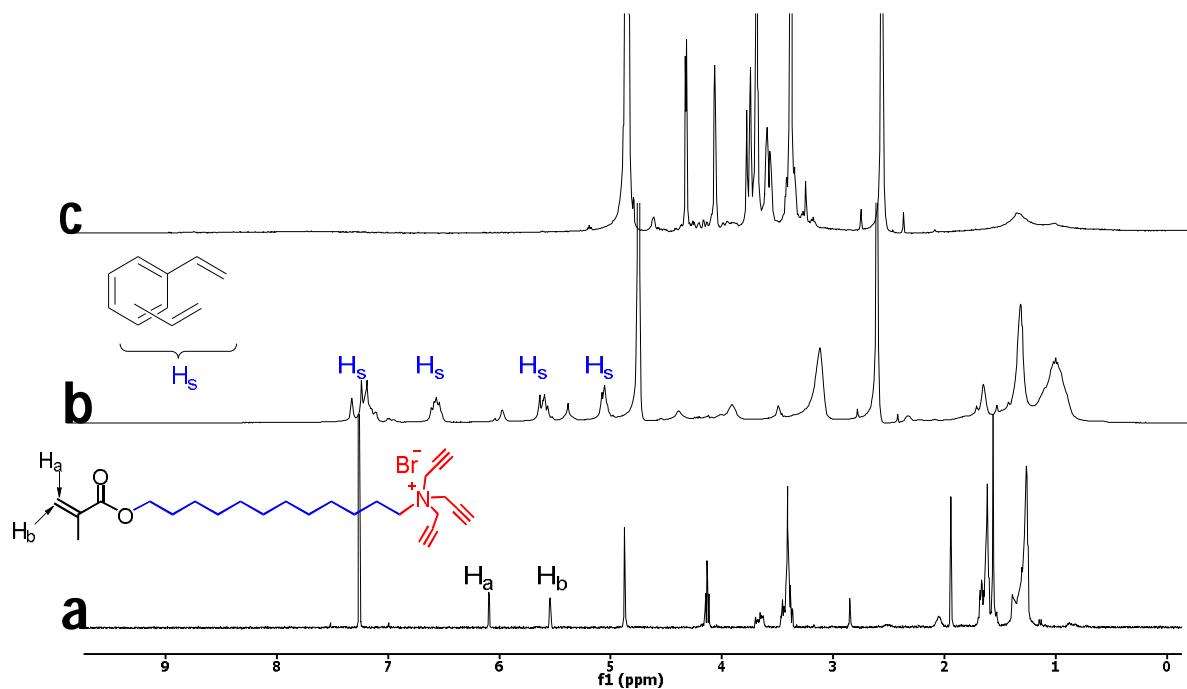


**Figure S28.**  $^1\text{H}$  NMR spectra of (a) Compound **1** in  $\text{CDCl}_3$ , (b) alkylnyl-SCM in  $\text{D}_2\text{O}$ , and (c) MINP(**6**) in  $\text{D}_2\text{O}$ .

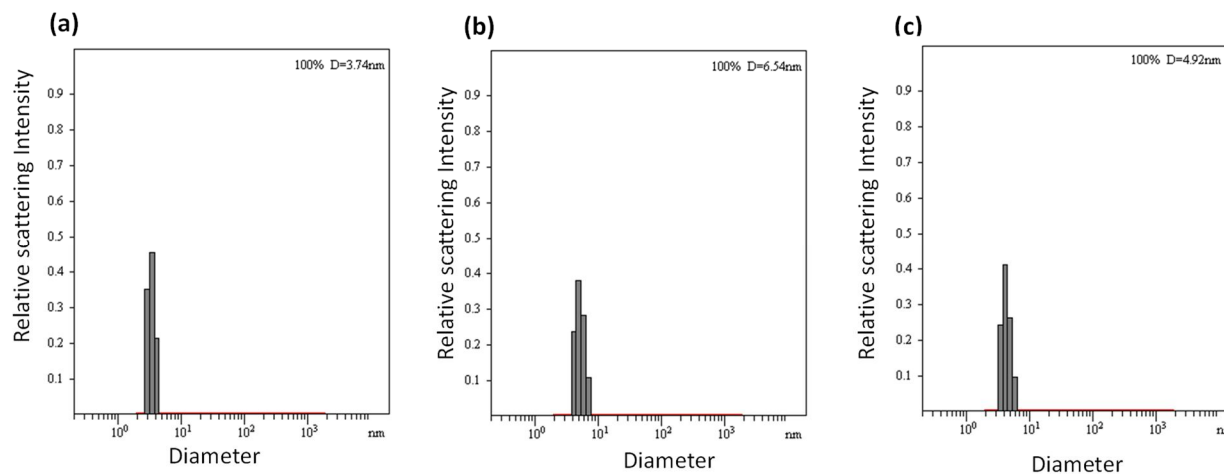


**Figure S29.** Distribution of the hydrodynamic diameters of the nanoparticles in water as determined by DLS for (a) alkylnyl-SCM, (b) surface-functionalized SCM, and (c) MINP(**6**) after purification.

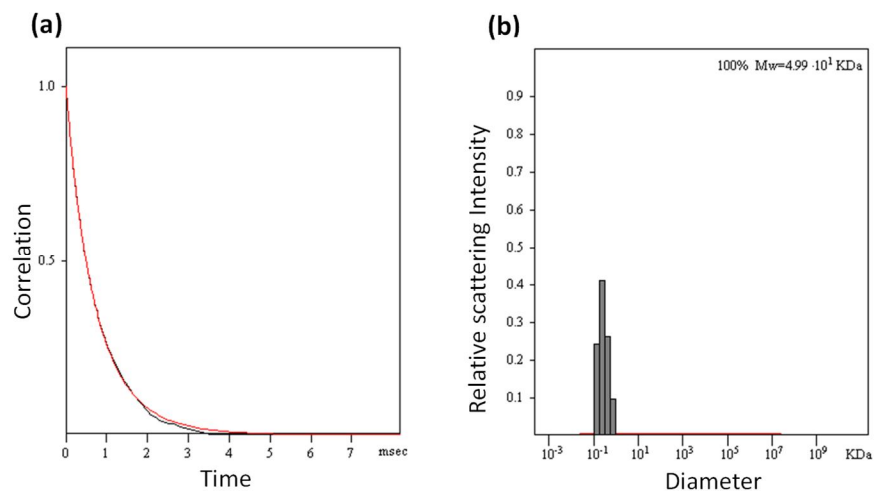


**Figure S30.** Distribution of the molecular weights and the correlation curves for MINP(**6**) from the DLS. The PRECISION DECONVOLVE program assumes the intensity of scattering is proportional to the mass of the particle squared. If each unit of building block for the MINP(**6**) is assumed to contain one molecule of compound **1** (MW = 465 g/mol), 1.2 molecules of compound **2** (MW = 172 g/mol), one molecule of DVB (MW = 130 g/mol), and 0.8 molecules of compound **3** (MW = 264 g/mol), the molecular weight of MINP(**6**) translates to 49 [= 49900 / (465 + 1.2×172 + 130 + 0.8×264)] of such units.

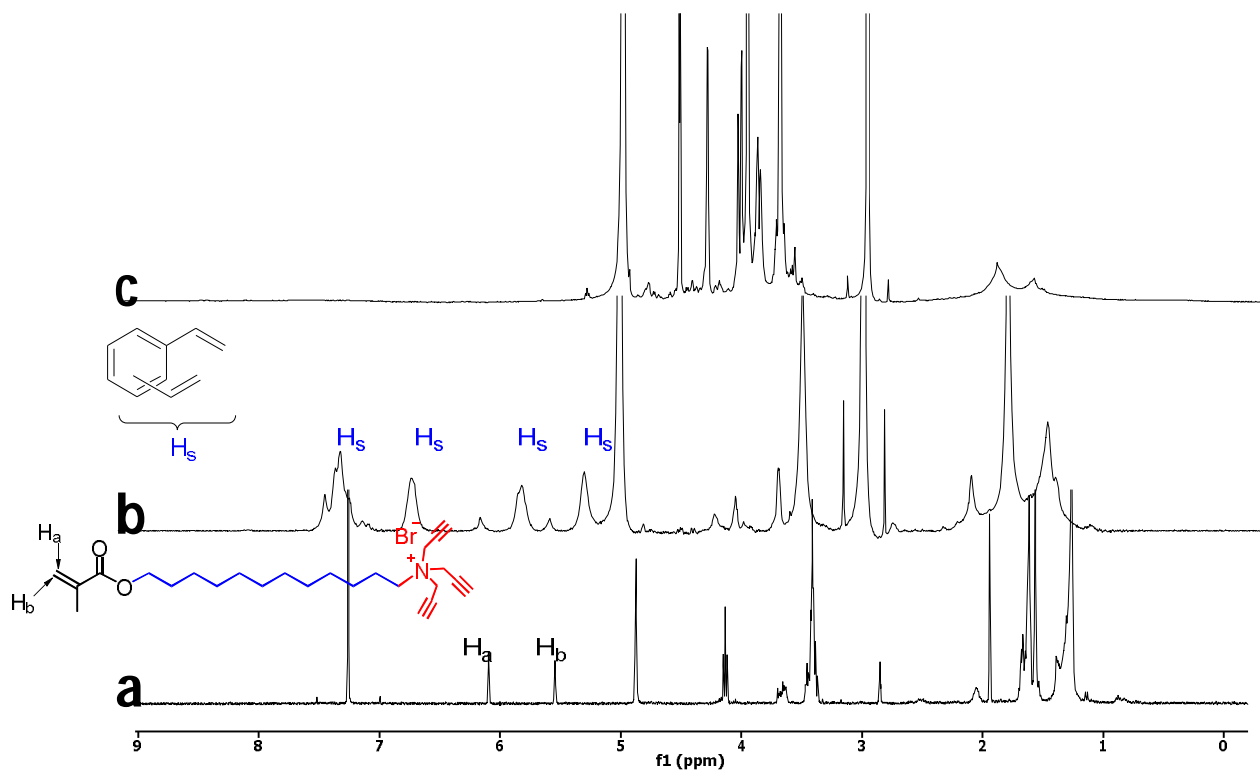


**Figure S31.**  $^1\text{H}$  NMR spectra of (a) Compound **1** in  $\text{CDCl}_3$ , (b) alkynyl-SCM in  $\text{D}_2\text{O}$ , and (c) MINP(7) in  $\text{D}_2\text{O}$ .

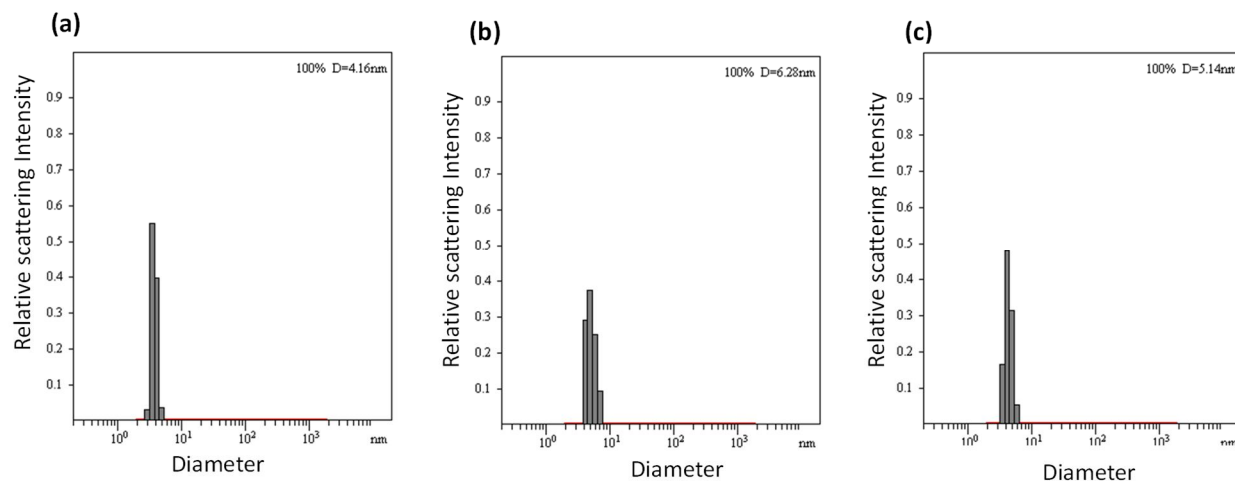


**Figure S32.** Distribution of the hydrodynamic diameters of the nanoparticles in water as determined by DLS for (a) alkynyl-SCM, (b) surface-functionalized SCM, and (c) MINP(7) after purification.

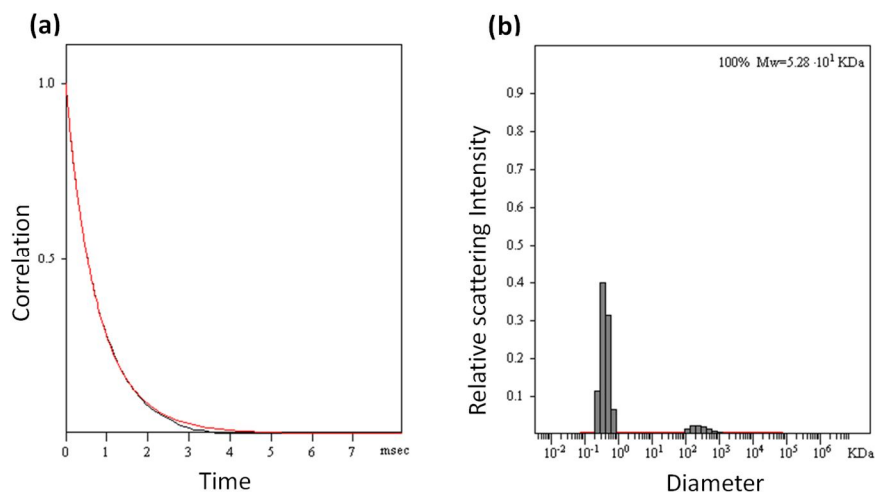


**Figure S33.** Distribution of the molecular weights and the correlation curves for MINP(7) from the DLS. The PRECISION DECONVOLVE program assumes the intensity of scattering is proportional to the mass of the particle squared. If each unit of building block for the MINP(7) is assumed to contain one molecule of compound **1** (MW = 465 g/mol), 1.2 molecules of compound **2** (MW = 172 g/mol), one molecule of DVB (MW = 130 g/mol), and 0.8 molecules of compound **3** (MW = 264 g/mol), the molecular weight of MINP(7) translates to 52 [= 52800 / (465 + 1.2 $\times$ 172 + 130 + 0.8 $\times$ 264)] of such units.

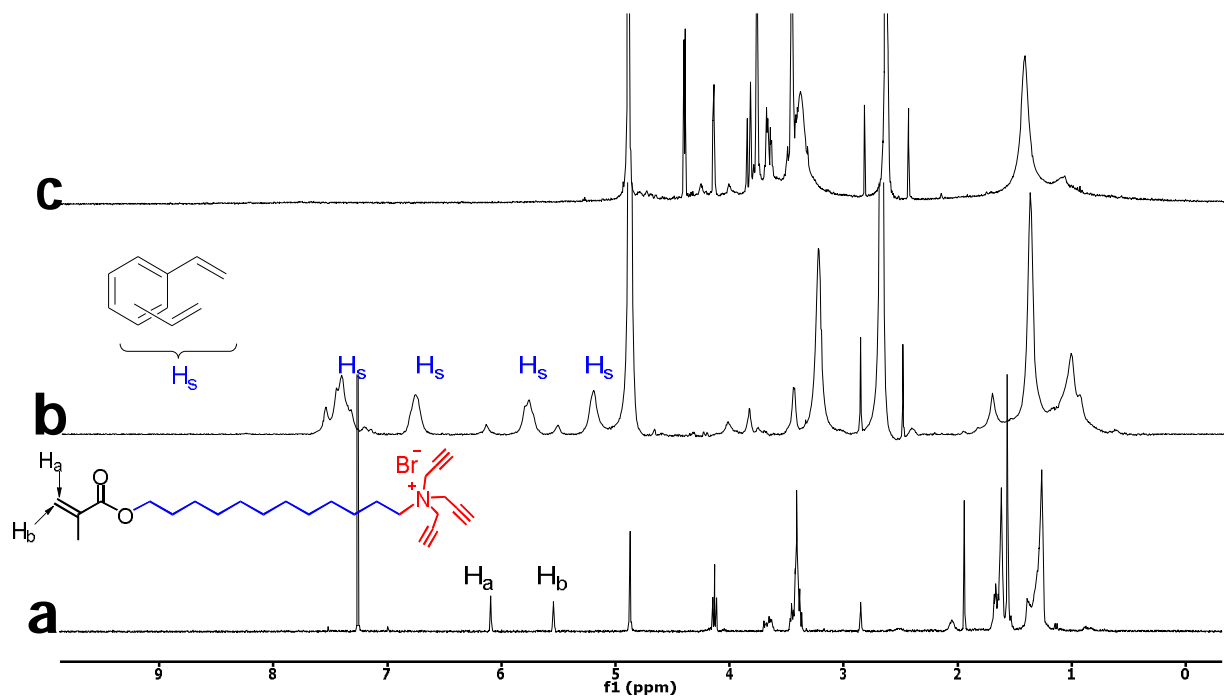


**Figure S34.**  $^1\text{H}$  NMR spectra of (a) Compound **1** in  $\text{CDCl}_3$ , (b) alkyne-SCM in  $\text{D}_2\text{O}$ , and (c) MINP(**8**) in  $\text{D}_2\text{O}$ .

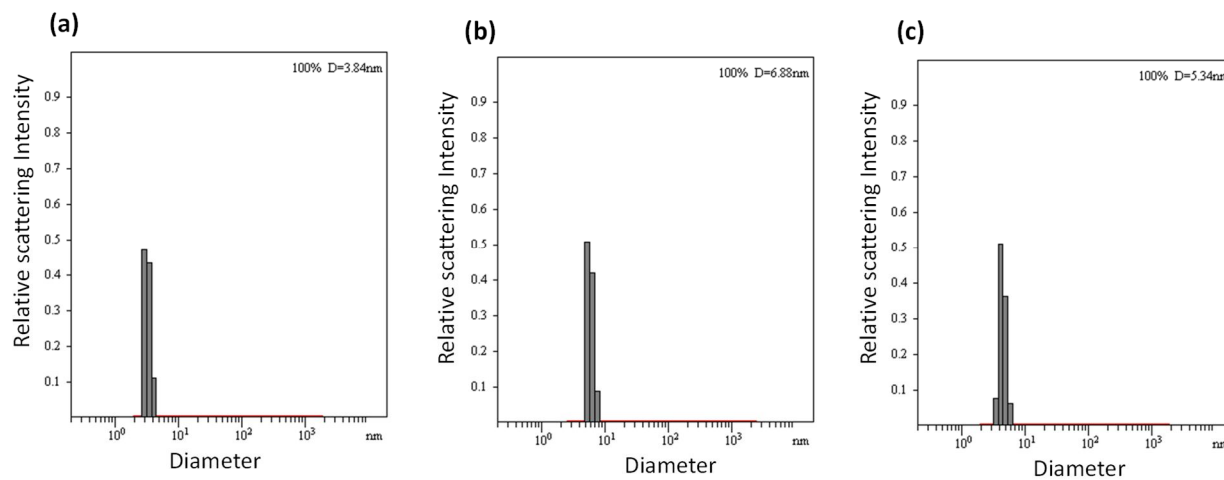


**Figure S35.** Distribution of the hydrodynamic diameters of the nanoparticles in water as determined by DLS for (a) alkyne-SCM, (b) surface-functionalized SCM, and (c) MINP(**8**) after purification.

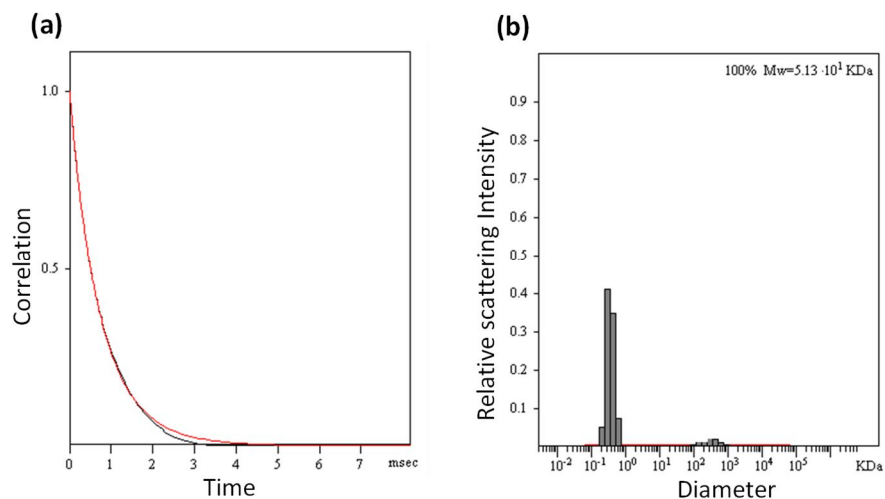


**Figure S36.** Distribution of the molecular weights and the correlation curves for MINP(**8**) from the DLS. The PRECISION DECONVOLVE program assumes the intensity of scattering is proportional to the mass of the particle squared. If each unit of building block for the MINP(**8**) is assumed to contain one molecule of compound **1** (MW = 465 g/mol), 1.2 molecules of compound **2** (MW = 172 g/mol), one molecule of DVB (MW = 130 g/mol), and 0.8 molecules of compound **3** (MW = 264 g/mol), the molecular weight of MINP(**8**) translates to 51 [= 51300 / (465 + 1.2×172 + 130 + 0.8×264)] of such units.

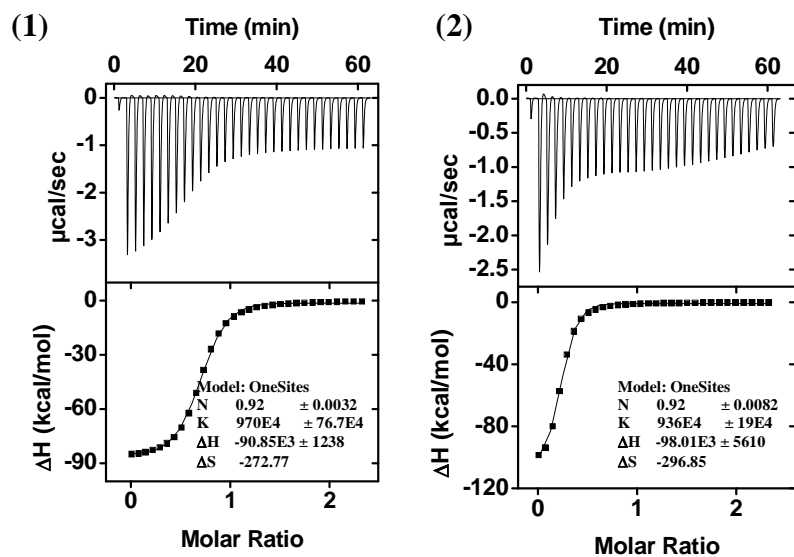


**Figure S37.** ITC titration curves obtained at 298 K for the titration of MINP(WWGG) (5  $\mu\text{M}$ ) with WWGG (50  $\mu\text{M}$ ) (a) Millipore water and (b) HEPES at pH 7.4. The data correspond to entries 1–2, respectively, in Table 1. The top panel shows the raw calorimetric data. The area under each peak represents the amount of heat generated at each ejection and is plotted against the molar ratio of MINP to the substrate. The solid line is the best fit of the experimental data to the sequential binding of N equal and independent binding sites on the MINP. The heat of dilution for the substrate, obtained by adding the substrate to the buffer, was subtracted from the heat released during the binding. Binding parameters were auto-generated after curve fitting using Microcal Origin 7.

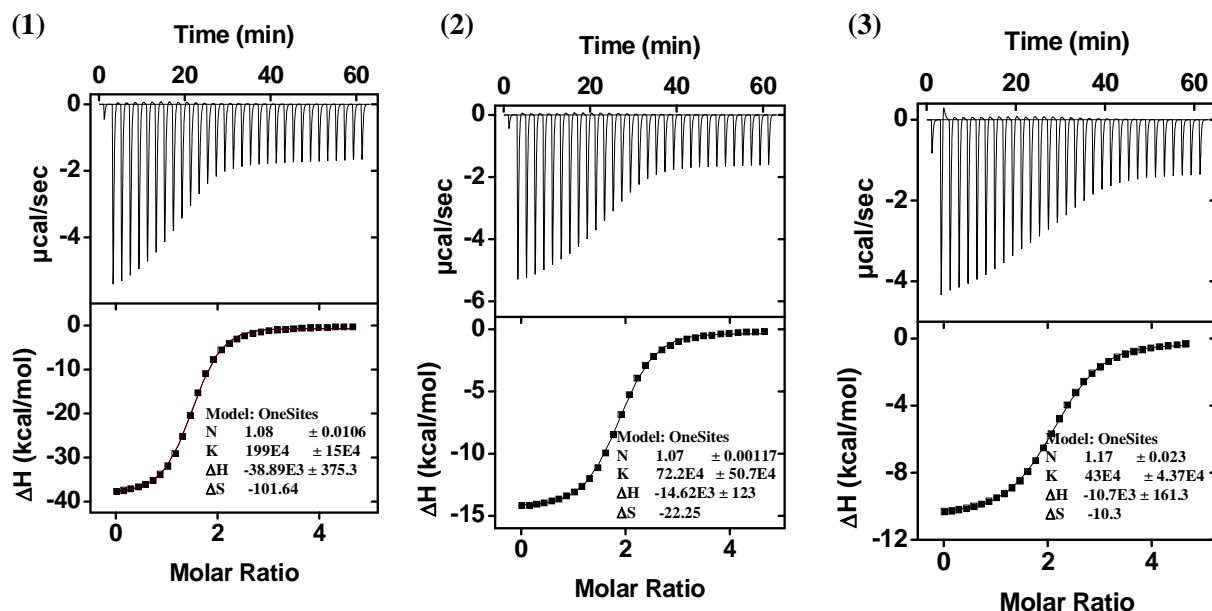


**Figure S38.** ITC titration curves obtained at 298 K for the titration of MINP(WWGG) (25 μM) with (a) GWWG (0.5 mM), (b) WGWG (0.5 mM), and (c) WGGW (0.5 mM) in Millipore water. The data correspond to entries 3–5, respectively, in Table 1. The top panel shows the raw calorimetric data. The area under each peak represents the amount of heat generated at each ejection and is plotted against the molar ratio of MINP to the substrate. The solid line is the best fit of the experimental data to the sequential binding of N equal and independent binding sites on the MINP. The heat of dilution for the substrate, obtained by adding the substrate to the buffer, was subtracted from the heat released during the binding. Binding parameters were auto-generated after curve fitting using Microcal Origin 7.

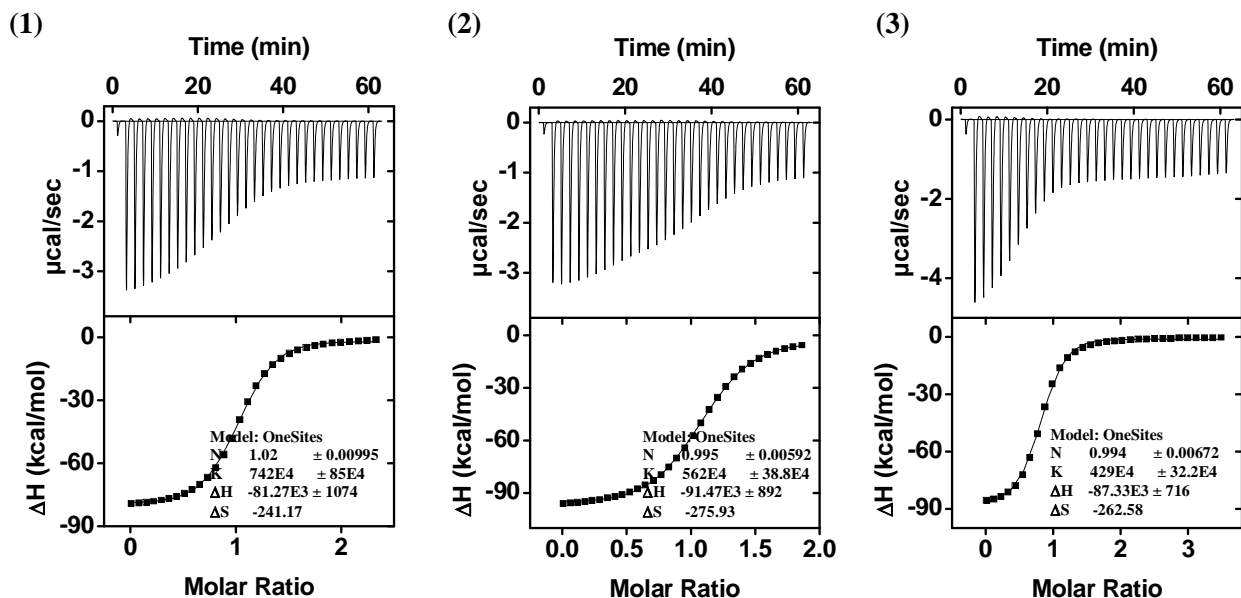


**Figure S39.** ITC titration curves obtained at 298 K for the titration of (a) MINP(GWWG) (6  $\mu\text{M}$ ) with GWGG (50  $\mu\text{M}$ ), (b) MINP(WGWW) (5  $\mu\text{M}$ ) with WGWW (40  $\mu\text{M}$ ), and (c) MINP(WGGW) (5  $\mu\text{M}$ ) with WGGW (50  $\mu\text{M}$ ) in Millipore water. The data correspond to entries 6–8, respectively, in Table 1. The top panel shows the raw calorimetric data. The area under each peak represents the amount of heat generated at each ejection and is plotted against the molar ratio of MINP to the substrate. The solid line is the best fit of the experimental data to the sequential binding of  $N$  equal and independent binding sites on the MINP. The heat of dilution for the substrate, obtained by adding the substrate to the buffer, was subtracted from the heat released during the binding. Binding parameters were auto-generated after curve fitting using Microcal Origin 7.

**Table S1: Fluorescence Binding Data.**

Entry	Host	Guest	$K_a$ ( $10^4 \text{M}^{-1}$ )
1	MINP(WWGG)	WWGG	914 $\pm$ 61
2	MINP(GWWG)	GWGG	786 $\pm$ 29
3	MINP(WGWW)	WGWW	638 $\pm$ 24
4	MINP(WGGW)	WGGW	480 $\pm$ 10

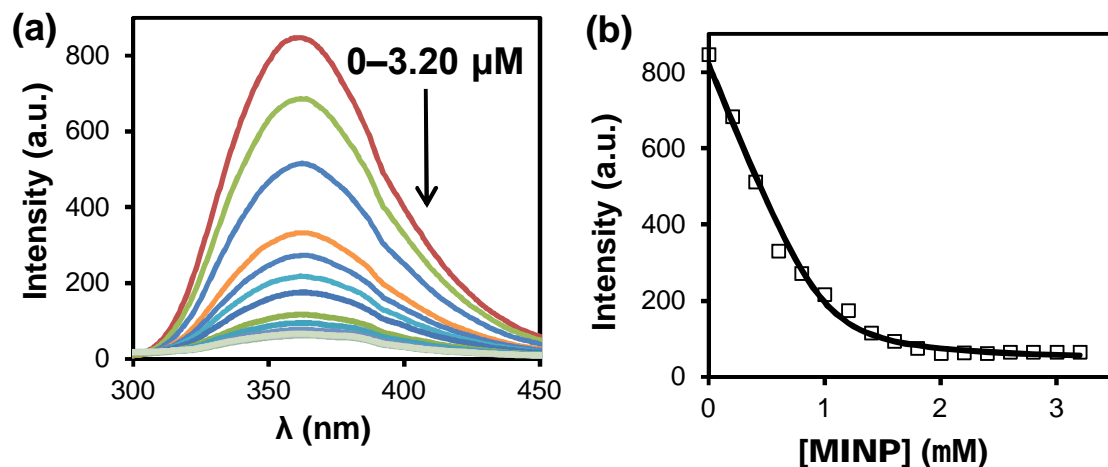


**Figure S40.** Fluorescence emission spectra of WWGG with different concentrations of MINP(WWGG) with an emission (a) ranging from 300 nm- 450 nm and (b) at 360 nm wavelength. The excitation wavelength ( $\lambda_{\text{ex}}$ ) is 280 nm and [WWGG] = 1.0  $\mu\text{M}$ . The data correspond to entry 1 in Table S1.

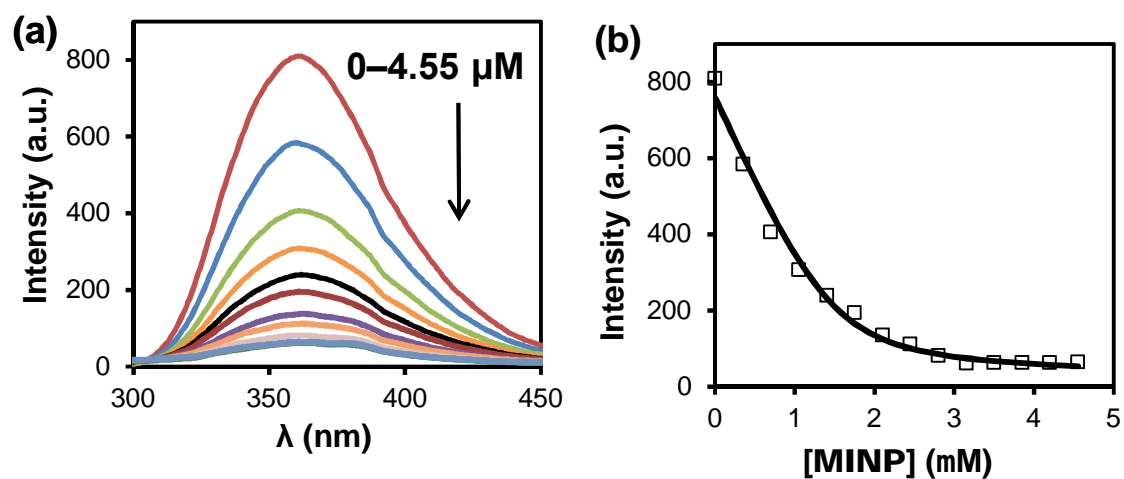


**Figure S41.** Fluorescence emission spectra of GWWG with different concentrations of MINP(GWWG) with an emission (a) ranging from 300 nm- 450 nm and (b) at 360 nm wavelength. The excitation wavelength ( $\lambda_{\text{ex}}$ ) is 280 nm and [GWWG] = 1.5  $\mu\text{M}$ . The data correspond to entry 2 in Table S1.

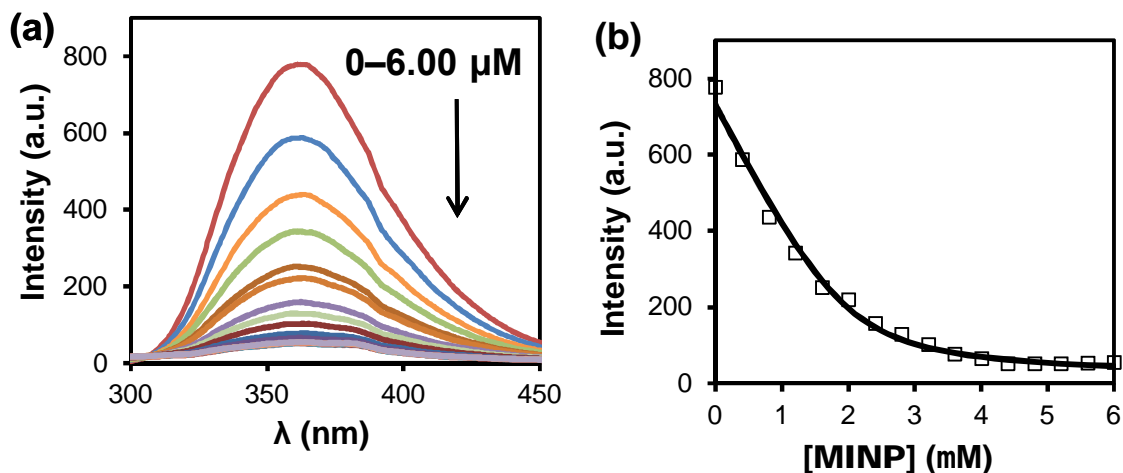


**Figure S42.** Fluorescence emission spectra of WGWG with different concentrations of MINP(WGWG) with an emission (a) ranging from 300 nm- 450 nm and (b) at 360 nm wavelength. The excitation wavelength ( $\lambda_{ex}$ ) is 280 nm and [WGWG] = 2.0 μM. The data correspond to entry 3 in Table S1.

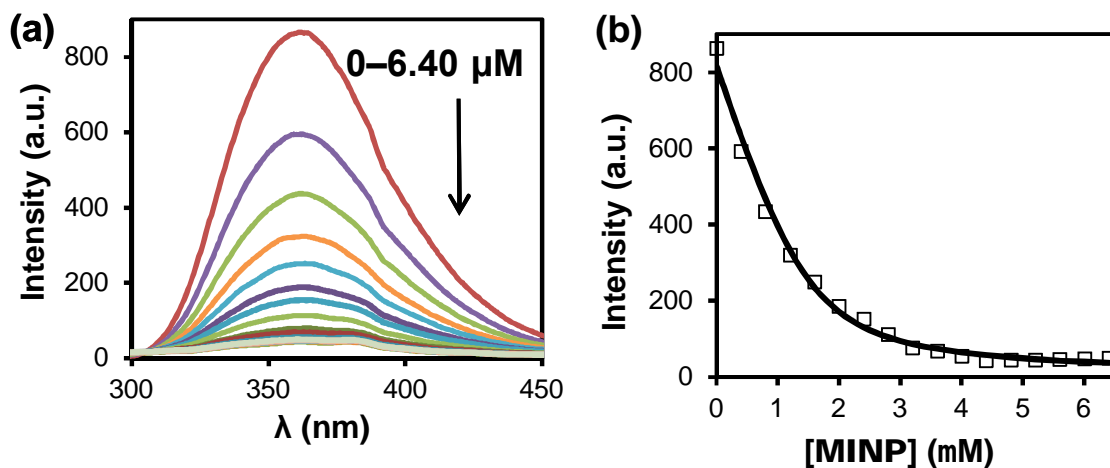


**Figure S43.** Fluorescence emission spectra of WGGW with different concentrations of MINP(WGGW) with an emission (a) ranging from 300 nm- 450 nm and (b) at 360 nm wavelength. The excitation wavelength ( $\lambda_{ex}$ ) is 280 nm and [WGGW] = 2.0 μM. The data correspond to entry 4 in Table S1.

**Table S2:** Job plot for the MINP(WWGG) ([H]) with different [WWGG] ([G]).

[G]/([G]+[H])	$\lambda_{em}=360\text{ nm}$ $F_{(Guest)}$	$\lambda_{em}=360\text{ nm}$ $F_{(H+G)}$	$\Delta F$
0.1	53.4	49.9	3.51
0.2	137.8	118.9	18.9
0.3	188.8	156.8	31.9
0.4	264.7	214.3	50.4
0.5	313.6	248.7	64.9
0.6	367.9	313.5	54.5
0.7	434.8	390.5	44.2
0.8	496.9	484.6	12.3
0.9	580.8	574.6	6.11

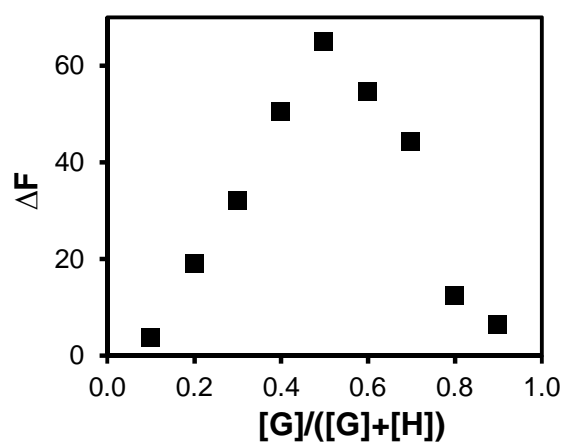


**Figure S44.** Job plot for the MINP(WWGG) with different molar ratio of [WWGG].

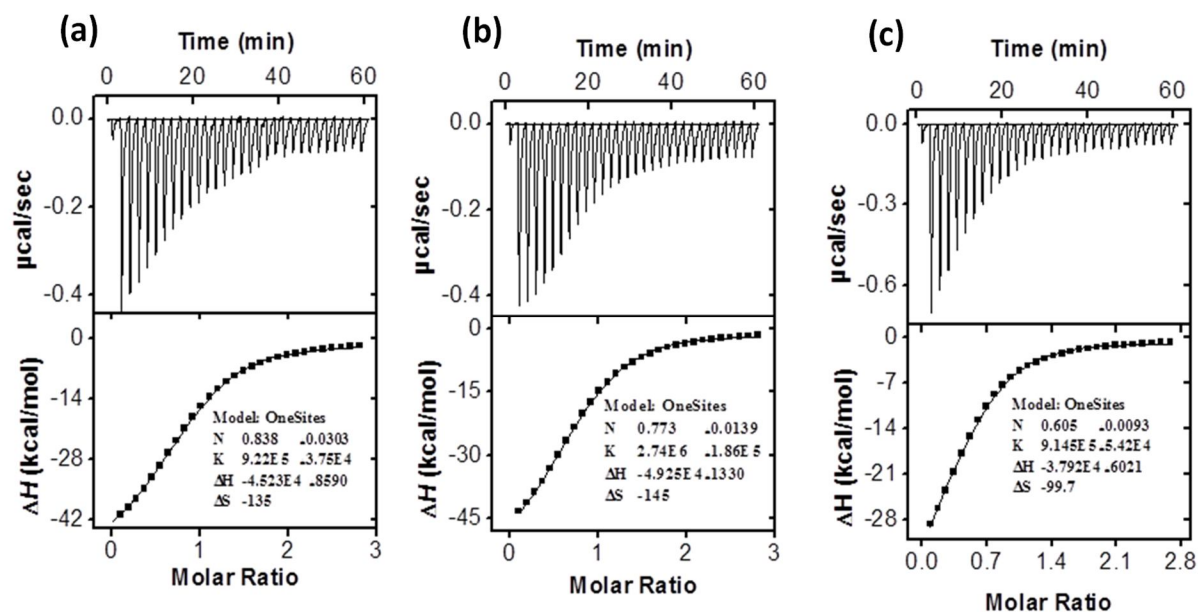


**Figure S45.** ITC titration curves obtained at 298 K for the binding of (a) FF (75  $\mu\text{M}$ ) by MINP(FF) (6.0  $\mu\text{M}$ ), (b) Boc-FF (60  $\mu\text{M}$ ) by MINP(Boc-FF) (5.0  $\mu\text{M}$ ), and (c) FGL (60  $\mu\text{M}$ ) by MINP(FGL) (5.0  $\mu\text{M}$ ). The data correspond to entries 1, 8, and 10 in Table 2, respectively. The top panel shows the raw calorimetric data. The area under each peak represents the amount of heat generated at each ejection and is plotted against the molar ratio of MINP to the substrate. The solid line is the best fit of the experimental data to the sequential binding of N equal and independent binding sites on the MINP. The heat of dilution for the substrate, obtained by adding the substrate to the buffer, was subtracted from the heat released during the binding. Binding parameters were auto-generated after curve fitting using Microcal Origin 7.

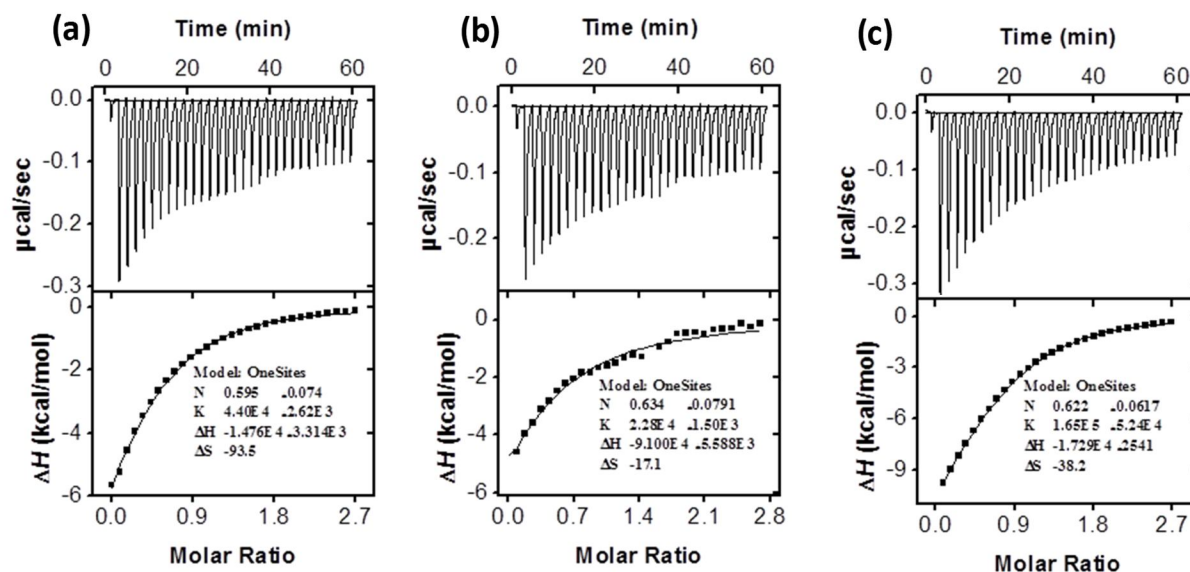


**Figure S46.** ITC titration curves obtained at 298 K for the binding of (a) FA (120  $\mu\text{M}$ ) by MINP(FF) (10  $\mu\text{M}$ ), (b) FI (120  $\mu\text{M}$ ) by MINP(FF) (10  $\mu\text{M}$ ), and (c) FL (60  $\mu\text{M}$ ) by MINP(FF) (5.0  $\mu\text{M}$ ). The data correspond to entries 2, 3, and 4 in Table 2, respectively. The top panel shows the raw calorimetric data. The area under each peak represents the amount of heat generated at each ejection and is plotted against the molar ratio of MINP to the substrate. The solid line is the best fit of the experimental data to the sequential binding of N equal and independent binding sites on the MINP. The heat of dilution for the substrate, obtained by adding the substrate to the buffer, was subtracted from the heat released during the binding. Binding parameters were auto-generated after curve fitting using Microcal Origin 7.

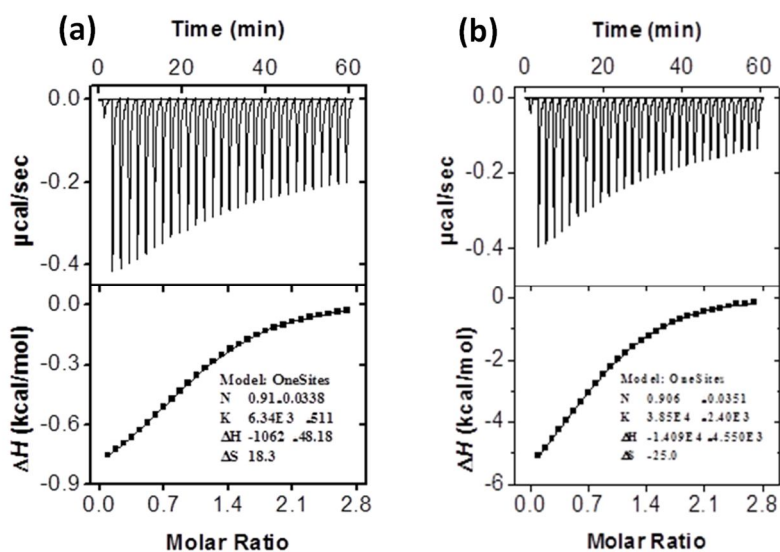


**Figure S47.** ITC titration curves obtained at 298 K for the binding of (a) FW (0.6 mM) by MINP(FF) (50  $\mu\text{M}$ ) and (b) FY (120  $\mu\text{M}$ ) by MINP(FF) (10  $\mu\text{M}$ ). The data correspond to entries 5 and 6 in Table 2, respectively. The top panel shows the raw calorimetric data. The area under each peak represents the amount of heat generated at each ejection and is plotted against the molar ratio of MINP to the substrate. The solid line is the best fit of the experimental data to the sequential binding of N equal and independent binding sites on the MINP. The heat of dilution for the substrate, obtained by adding the substrate to the buffer, was subtracted from the heat released during the binding. Binding parameters were auto-generated after curve fitting using Microcal Origin 7.

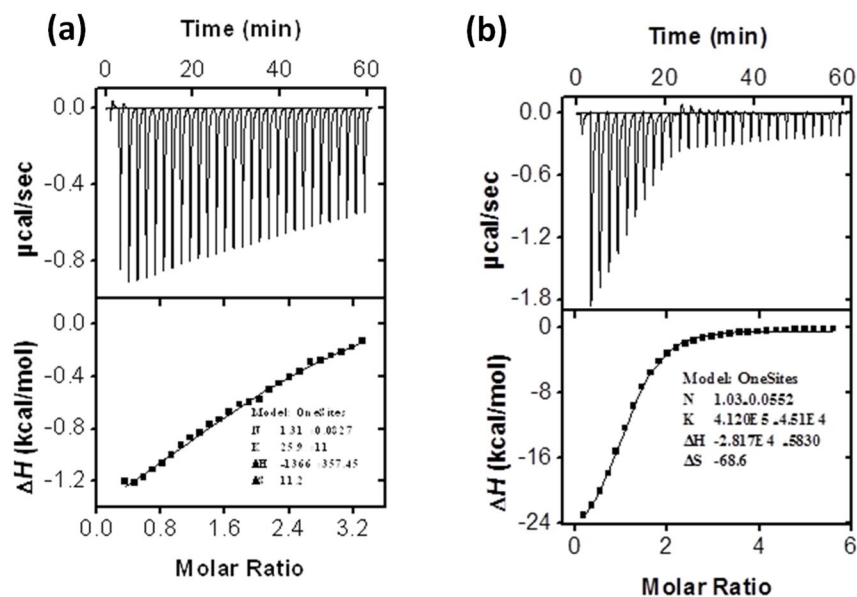


**Figure S48.** ITC titration curves obtained at 298 K for the binding of (a) Boc-FF (0.8 mM) by MINP(FF) (50 μM), (b) FF (250 μM) by MINP(Boc-FF) (10 μM). The data correspond to entries 7 and 9 in Table 2, respectively. The top panel shows the raw calorimetric data. The area under each peak represents the amount of heat generated at each ejection and is plotted against the molar ratio of MINP to the substrate. The solid line is the best fit of the experimental data to the sequential binding of N equal and independent binding sites on the MINP. The heat of dilution for the substrate, obtained by adding the substrate to the buffer, was subtracted from the heat released during the binding. Binding parameters were auto-generated after curve fitting using Microcal Origin 7.

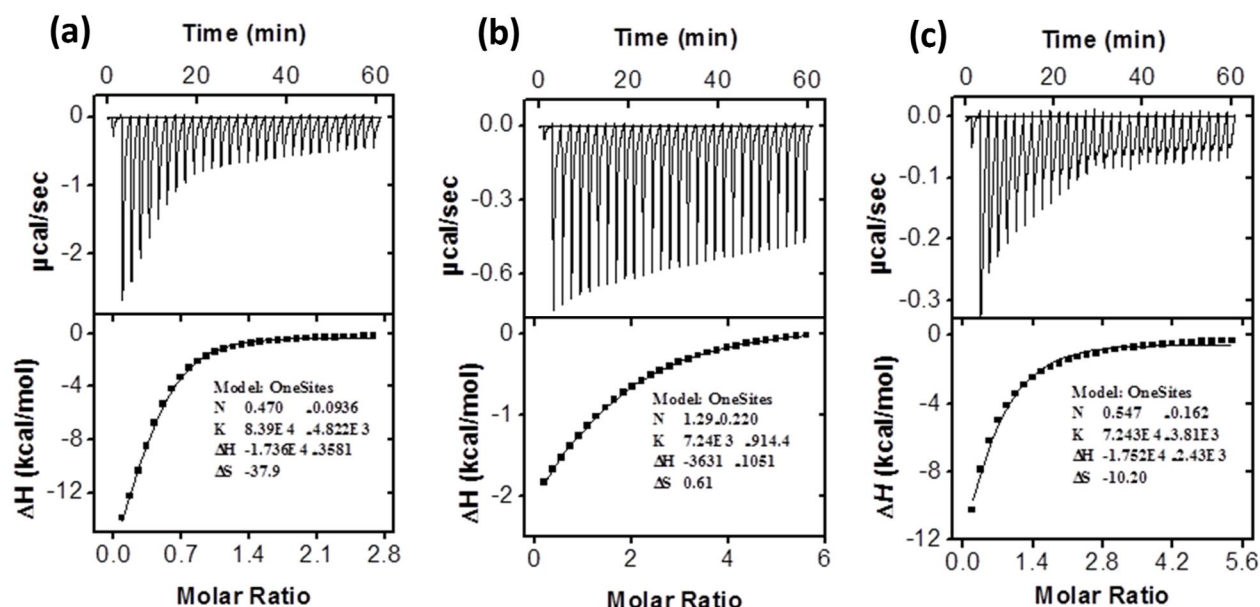


**Figure S49.** ITC titration curves obtained at 298 K for the binding of (a) FGI (0.6 mM) by MINP(FGL) (50  $\mu\text{M}$ ), (b) FLG (0.5 mM) by MINP(FGL) (20  $\mu\text{M}$ ), and (c) FGGL (0.12 mM) by MINP(FGL) (5.0  $\mu\text{M}$ ). The data correspond to entries 10, 11, and 12 in Table 2, respectively. The top panel shows the raw calorimetric data. The area under each peak represents the amount of heat generated at each ejection and is plotted against the molar ratio of MINP to the substrate. The solid line is the best fit of the experimental data to the sequential binding of N equal and independent binding sites on the MINP. The heat of dilution for the substrate, obtained by adding the substrate to the buffer, was subtracted from the heat released during the binding. Binding parameters were auto-generated after curve fitting using Microcal Origin 7.

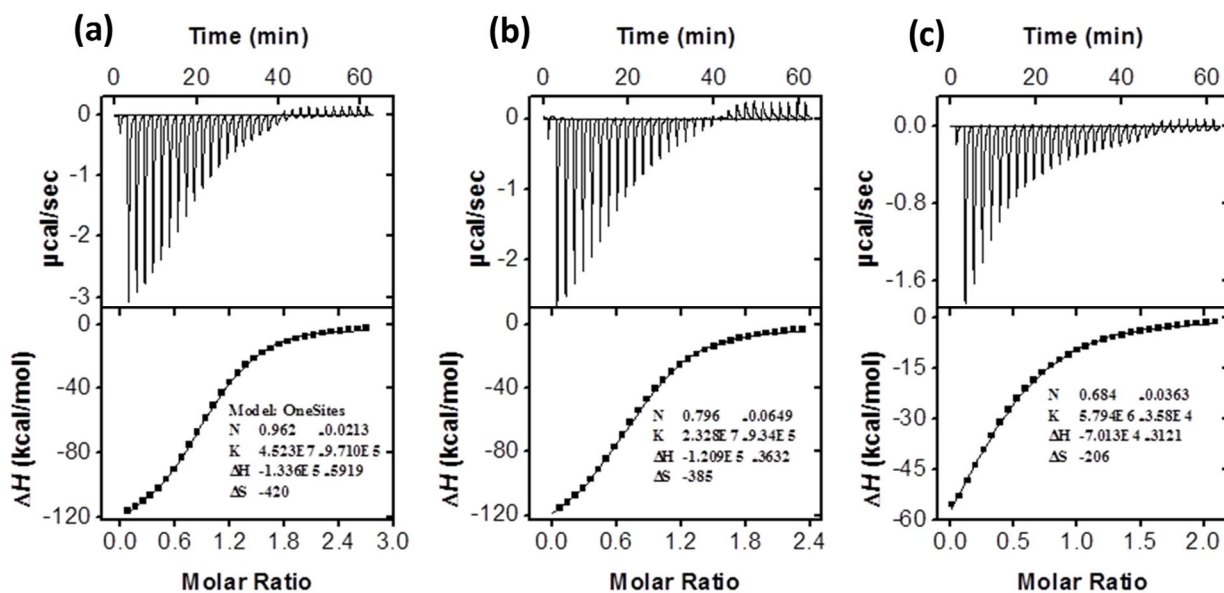


**Figure S50.** ITC titration curves obtained at 298 K for the binding of (a) **4** (70  $\mu\text{M}$ ) by MINP(**4**) (6.0  $\mu\text{M}$ ), (b) **5** (60  $\mu\text{M}$ ) by MINP(**5**) (6.0  $\mu\text{M}$ ), and (c) **6** (90  $\mu\text{M}$ ) by MINP(**6**) (10  $\mu\text{M}$ ). The data correspond to entries 14, 15, and 16 in Table 2, respectively. The top panel shows the raw calorimetric data. The area under each peak represents the amount of heat generated at each ejection and is plotted against the molar ratio of MINP to the substrate. The solid line is the best fit of the experimental data to the sequential binding of  $N$  equal and independent binding sites on the MINP. The heat of dilution for the substrate, obtained by adding the substrate to the buffer, was subtracted from the heat released during the binding. Binding parameters were auto-generated after curve fitting using Microcal Origin 7.

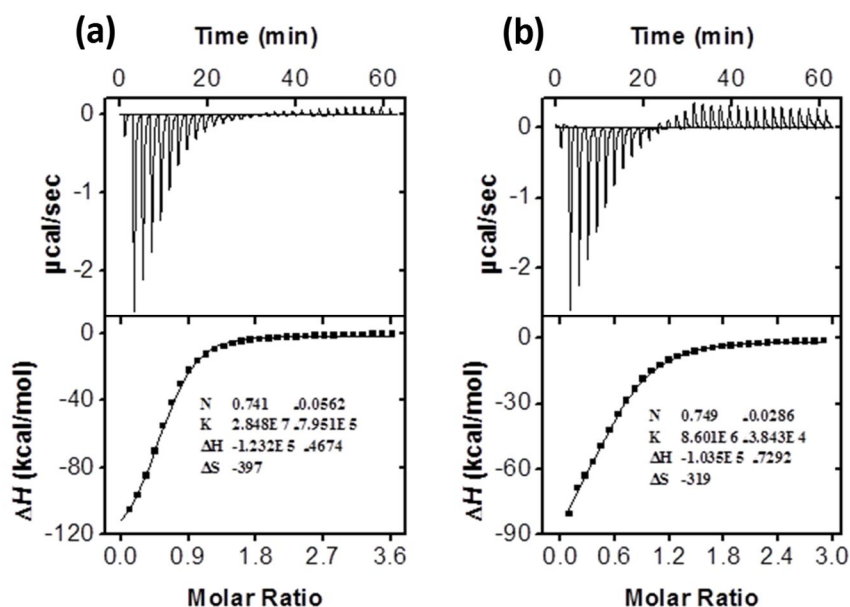


**Figure S51.** ITC titration curves obtained at 298 K for the binding of (a) **7** (70 μM) by MINP(**7**) (5.0 μM) and (b) **8** (100 μM) by MINP(**8**) (8.0 μM). The data correspond to entries 17 and 18 in Table 2, respectively. The top panel shows the raw calorimetric data. The area under each peak represents the amount of heat generated at each ejection and is plotted against the molar ratio of MINP to the substrate. The solid line is the best fit of the experimental data to the sequential binding of N equal and independent binding sites on the MINP. The heat of dilution for the substrate, obtained by adding the substrate to the buffer, was subtracted from the heat released during the binding. Binding parameters were auto-generated after curve fitting using Microcal Origin 7.

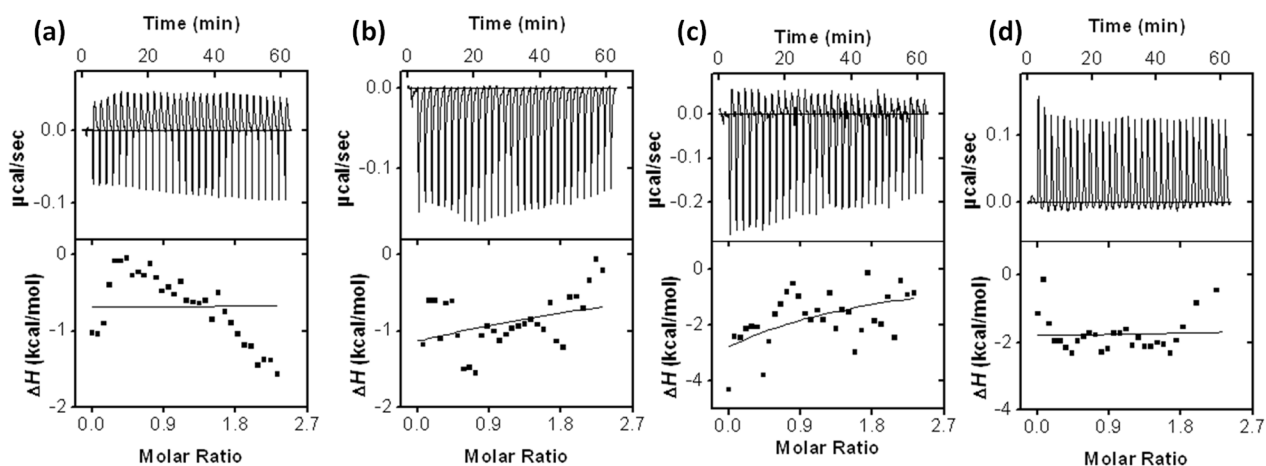


**Figure S52. Cross reactivity studies:** ITC titration curves obtained at 298 K for the binding of **4** (a), **6** (b), **7** (c), and **8** (d) by MINP(**5**). The concentration of each guest was ( $60 \mu\text{M}$ ) while that of MINP(**5**) was  $6.0 \mu\text{M}$ . The top panel shows the raw calorimetric data. The area under each peak represents the amount of heat generated at each ejection and is plotted against the molar ratio of MINP to the substrate. The solid line is the best fit of the experimental data to the sequential binding of  $N$  equal and independent binding sites on the MINP. The heat of dilution for the substrate, obtained by adding the substrate to the buffer, was subtracted from the heat released during the binding. Binding parameters were auto-generated after curve fitting using Microcal Origin 7.

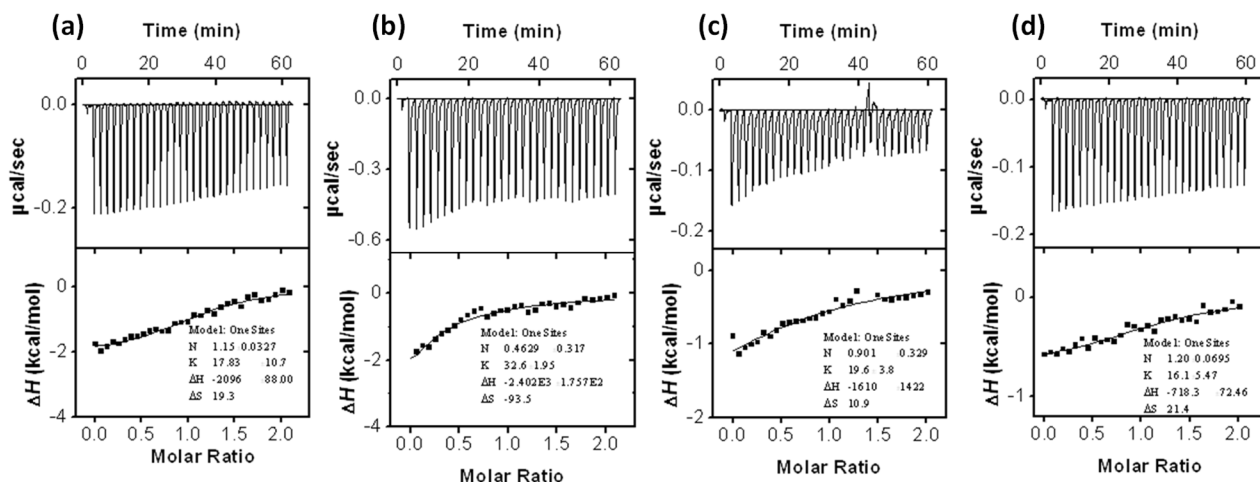


**Figure S53. Cross reactivity studies:** ITC titration curves obtained at 298 K for the binding of **6** by (a) MINP(**4**), (b) MINP(**5**), (c) MINP(**7**), and (d) MINP(**8**). The concentration of the guest was (90  $\mu$ M) and that of each MINP was 10  $\mu$ M. The top panel shows the raw calorimetric data. The area under each peak represents the amount of heat generated at each ejection and is plotted against the molar ratio of MINP to the substrate. The solid line is the best fit of the experimental data to the sequential binding of N equal and independent binding sites on the MINP. The heat of dilution for the substrate, obtained by adding the substrate to the buffer, was subtracted from the heat released during the binding. Binding parameters were auto-generated after curve fitting using Microcal Origin 7.